Ecology and evolution in fluctuating environments

A Thesis
SUBMITTED TO THE FACULTY OF
UNIVERSITY OF MINNESOTA
BY

Xiao Yi

IN PARTIAL FULFILLMENT OF THE REQUIREMENTS
FOR THE DEGREE OF
DOCTOR OF PHILOSOPHY

Advisor: Antony Dean

September 2015

Acknowledgements

In the course of past seven years, I have experienced an intense and unique trajectory in the exploration of scientific curiosity. This journey would have been impossible without the tremendous help from the following individuals.

I am indebted to my advisor Dr. Antony Dean for recruiting me to his laboratory and allowing me the freedom to let my imagination take off. I thank my committee members, Drs. Michael Travisano, R. Ford Denison and Claudia Schmidt-Dannert, for providing feedbacks to this thesis. I thank Dr. William Ratcliff for his encouragement and serving as a role model. I thank members from the Dean laboratory, Dr. Stephen Miller and Mark Lunzer, for discussion on experiments and techniques. I thank the undergraduate students I have advised, Suyang Wan and Austin Cole, for brainpowering with me in the development of some research ideas.

Also, there are people with whom I have not been in daily contact but who have provided critical advice or influence. I am grateful to Dr. Stanislas Leibler from Rockefeller University, whose work has inspired my interest in evolution in changing environments and whose style has deeply influenced my taste of science. I thank Dr. Sunney Xie from Harvard University and Dr. Long Cai from California Institute of Technology for suggesting the phase variation based mechanism of bistable gene expression, which became the cornerstone of my bet-hedging project. My thanks also go to Dr. Gaowei Wang from Shanghai Jiaotong University for sharing insights on quantitative approach to biological problems.

Dedication

This thesis is dedicated to my farther, without whom I would have been long lost in this confusing world.

Abstract

Temporally variable environments are the norm rather than the exception in nature. Yet, the ecological consequences of this variability and the evolutionary responses it invokes remain poorly understood. In this thesis, a previously proposed theory of competitive coexistence was further developed that yielded a nonconventional prediction: fluctuating environments can support stable coexistence of competitors even in the absence of negative frequency-dependent selection. It was confirmed by laboratory competition using bacteria. After generalization of the theory by simulation, an alternative to the genetic drift model emerges that explains the rich polymorphism observed in nature. Next, a dynamic theory of bet-hedging was developed and tested by experiments, which also proved stochastic phenotypic switching as a highly adaptive bet-hedging strategy. Besides, this new theory predicts that the standard theory of bet-hedging should fail under certain conditions of direct biological relevance. With the ecological and evolutionary models tested, a forward evolutionary experiment was carried out to study adaptation to fluctuating environments. Hypothesis free, this effort captured unexpected strategies to cope with cyclic environments, revealing the generative effect of trade-off in the presence of two-dimensional selection. Together, these three projects offer a multi-perspective picture of the complex process of adaptation in fluctuating environments, with an emphasis on mechanisms—ecological or physiological—that underlie the emergence of varied evolutionary responses.

Table of contents

List of Tables

List of Figures

Chapter 1

Introduction

1.1 General background

Organisms are constantly challenged by temporal changes of the environment (Bell, 2010). This variability imposes as profound restraints for the prosperity of organisms as it provides unique opportunities for the emergence of biological complexities such as bet-hedging behavior. For pathogenic bacteria, the dynamic environment of human body changes on the scale of minutes due to the rapid innate immune response (Domínguez et al., 2003). For short-lived insects, hourly varying temperature in the wild plays an essential role in shaping their life history (Brittain and Campbell, 1991). For plants, seasonal fluctuations in sun light, nutrients, etc. introduce rhythm as well as stochasticity to the demographic and population processes (Pake and Venable, 1996).

The topic of variable environments has been researched at different levels (Chesson and Huntly, 1993; Frank and Slatkin, 1990). At the ecological level, where a community of multiple species is concerned, environmental change across time shapes the population dynamics of competing species. Three distinct fates are possible for each species: taking over the community, extinction or stable coexistence with the rest of the community. For instance, coexistence of multiple species becomes possible when trade-off is present (Chesson, 2000). Here each competitor has some bad times with low fitness, but also has some good times with high fitness. As the environment shifts between good and bad times, it becomes difficult for any single species to take over the community.

At the evolutionary level, focus is directed towards genetic polymorphism within populations as well as adaptive strategies to maintain/increase fitness in the face of environmental variability . Theoretical (Cohen, 1966; Dempster, 1955; Haldane and Jayakar, 1963) and empirical (Levin, 2000; Philippi, 1993; Simons, 2009; Suiter et al., 2003) studies have outlined the principles underlying the evolutionary responses to changing environments. Different patterns of environmental change select for different strategies (Kussell and Leibler, 2005). Responsive sensing allows organisms to respond to environmental signals that indicate forthcoming changes (e.g. shortening daylight hours are a harbinger that winter will soon arrive). When the changes are unpredictable , bet-hedging may be favored (Beaumont et al., 2009; Levin, 1968). With such strategy, a population stochastically partitions into multiple subgroups, each of a different phenotypic state that fits one environmental condition (Acar et al., 2008; Thattai and van Oudenaarden, 2004). Consequently, there is always a subgroup of individuals that fit the incoming environmental change, thereby preventing the population from extinction.

Despite intensive efforts that have been made on examining the effects of temporal variations of environment at both the ecological and evolutionary levels (Chesson and Huntly, 1993; Dempster, 1955; Simons, 2009; Turelli et al., 2001b), previous work is either purely theoretical or based on field observation: rigorous test of models with controlled experiments is lacking.

1.2 Competitive coexistence in changing environments

Ever since its proposal by G. Evelyn Hutchinson (Hutchinson, 1961), the paradox of plankton—the enormous range of plankton species despite the poor nutrition conditions in the ocean—inspired an army of researchers to pursue the topic of biodiversity. Spatial heterogeneity is an intuitive mechanism that supplies large number of niches for life to specialize upon (Tamme et al., 2010) and has been widely recognized as a primary contributor to diversity (Simon, 1976). Temporal heterogeneity, nonetheless, has been deemed important only by some (Chesson, 1983) but trivial by the mass majority of biologists (Dempster, 1955; Schoener, 1974).

The controversy arises from ambiguity in the varied setup of the models used by different authors, which reflects diverse ways temporal variability can influence competition dynamics. For instance, stable coexistence of multiple competitors can be maintained by varying growth rate and death rate across a serial bouts of competition in a lottery model (Chesson, 1983). In each bout, a fraction of the fully occupied habitats are chosen for clearance by death; the remaining individuals compete for these freed spots according to their growth rates. Such model simulates a highly competitive and crowded environment, such as tropic rain forest ecosystem, and thus inherits negative frequency-dependent growths: as the advantageous competitor increases frequency in the community, its gain diminishes due to the fixed capacity of the habitats and the relative nature of competition.

Then again, competitive coexistence is not possible in a model where competitors simply grow by randomly assigned growth rates without interacting with each other

(Dempster, 1955). Negative frequency-dependence absent, this model assumes abundant resources, and competitors composition of the population is subject to random drift, leading to eventual extinction of some species.

1.3 Standard theory of bet-hedging

A risk-reducing strategy in the face of uncertainty, bet-hedging is central to the studies of adaptation to changing environments (Simons, 2009). In a typical situation, organisms are propagating through a sequence of environments, each specifying a different level of fitness due to fluctuating conditions such as seasonality. Technically, bet-hedging is defined by the maximization of geometric mean of all local fitnesses in each environment at the expense of the arithmetic mean (Starrfelt and Kokko, 2012). Intuitively, it means the long-term (geometric mean) fitness is evolutionarily important and needs to be optimized, overriding the short-term benefit (arithmetic mean fitness). Significance of this principle is best illustrated from the opposite: imagine fitness becomes zero in one of the environments. This extreme fitness value will not disrupt the arithmetic mean because its negative effect is diluted by summation across all environments; to the contrary, it crushes the geometric mean to zero by rule of multiplication, signifying the worst scenario of extinction.

The means to change and optimize geometric mean fitness is to diversify the phenotypes or behaviors spontaneously and stochastically, provided that there is no signal to predict forthcoming change of environment. Examples include annual plants produce seeds in a dispersed range of time in a year (Pake and Venable, 1996); bacteria

dynamically switch on and off their motility (Koirala et al., 2014); growth rates of an isogenic yeast population demonstrate bimodal distribution (Levy et al., 2012).

Bet-hedging has been investigated with different types of models: continuous time, where growth and phenotypic diversification within and across environments are modeled explicitly by differential equations (Kussell and Leibler, 2005), such as for bacterial motility; or discrete time, where within-environment dynamics are ignored, leaving inter-environment variations to the focus (Simons, 2009), such as for annual plants' seed bank. Distinct as they are in formulation, both models come to the same conclusion: when the phenotypic switching rate matches the environmental shifting rate, the geometric mean fitness will hit optimum (Kussell and Leibler, 2005; Simons, 2009). The reason is that this match minimizes variance among local fitnesses. Mathematically, the global geometric mean fitness is maximized at the same time. (Starrfelt and Kokko, 2012).

1.4 Summary

Apparent from previous two sections, ecology and evolution in fluctuating environments are highly dynamic in both biotic and abiotic components and multivariate in the determination of competition outcome, leaving the gap between theories and observed phenomena still wide open.

Fortunately, recent development in the engineering field of synthetic biology has started to provide new experimental tools cogently needed. Examples include precise phenotypic programming in microbes using genetic circuit (Friedland et al., 2009) and

automated experimental platforms with standardized control (Toprak et al., 2012) or high-throughput capacity (Wang et al., 2009).

The initial goal of my thesis research is to develop a new model of competitive coexistence and test with experiments; then test bet-hedging theory with direct measurements using carefully engineered bacteria. The challenge to achieving this goal is construction of a reliable competition system amenable to convenient manipulation. Not only does such a system require organisms to have predictable phenotypes with desired fitness consequence, but their behavior—dynamic switching between the phenotypes—in a fluctuating environment should be consistent and under control. In order to address this challenge, synthetic biology approach was taken to engineer strains of bacteria that carry sophisticated genetic circuits that generate controlled dynamic behaviors. After a large amount of trial-and-error and painstaking characterization, an experimental system that fulfills the requirements was complete, consisting of precisely engineered bacterial strains and fully controlled fluctuating environments in the laboratory.

While the initial goal is addressed through hypothesis testing with experimental systems that are built bottom-up, the second goal of my thesis is to explore to a fuller extent the complexity in adaptation to fluctuating environments by means of top-down experiments. Instead of concentrating on specific types of strategies, bacteria were evolved in a cyclic environment for many generations, allowing any adaptive strategies to occur freely. Mutants isolated along the evolutionary progression were systematically characterized to identify genetic cause of adaptation. Candidates were analyzed by sequencing, genetics and phenotypic assays to determine the mechanisms. This approach

complements the bottom-up approach by capturing alternative scenarios that are neglected in standard model or violate its assumptions.

Chapter 2

Ecological conditions for competitive coexistence

Understanding the mechanisms maintaining biological diversity remains a major challenge in ecology and population genetics. While the role of spatial heterogeneity in promoting biological diversity is widely recognized (Amarasekare, 2003; Schoener, 1974), that played by temporal fluctuations in selection has received less attention. Ecologists suggest environmental fluctuations promote diversity by reducing competition through a temporal partitioning of resource use(Cáceres, 1997; Pake and Venable, 1996; Turelli et al., 2001a), although in many models frequency-dependent growth rates allow stable coexistence even in constant environments (e.g. the Lotka-Volterra competition model(Gotelli, 2008)). Explicit tests of ecological coexistence theory are scant(Codeço and Grover, 2001; Siepielski and McPeek, 2010).

Population genetic theory predicts competitors (species or genetic clones) cannot coexist in a fluctuating environment unless relative fitness is frequency-dependent (Dempster, 1955; Felsenstein, 1976; Kimura, 1954; Stewart and Levin, 1973). Frequency-dependent selection is defined as the dependence of a competitor 's relative fitness (relative growth rate) on its frequency in the total population(Heino et al., 1998). Although some polymorphisms are maintained by frequency-dependent selection, most are not (Mitchell-Olds, 2007). In the absence of frequency-dependent selection population genetic theory predicts the clone with the largest geometric mean fitness always sweeps to fixation (Dempster, 1955).

Consensus about the importance of fluctuating selection and the mechanism by which it does, or does not, maintain biological diversity is lacking. Here, we demonstrate that fluctuating selection can maintain biological diversity in the absence of frequency-dependent selection.

2.1 Model

Consider two competing populations inhabiting a seasonal environment of growth, in which finite resources become depleted, followed by death prior to the cycle repeating. Let $d_{x.i}$ be the number of population doublings by competitor *x* in season *i*, and assume that deaths are random so that only a fraction of the total population survives to the next cycle. A rare competitor *A* increases in frequency across multiple growth seasons when its doublings exceed those of the common competitor *a*, $\sum_{i=1}^{n} d_{A.i} > \sum_{i=1}^{n} d_{a.i}$. In a serial transfer experiment each $2^{d_{a.i}}$ of the common competitor equals the daily dilution factor (usually 100-fold). With $d_{a.i}/\sum_{i=1}^{n} d_{a.i} = 1/n$, the condition for *A* to increase in frequency is that its arithmetic mean relative fitness be greater than one

$$\frac{1}{n}\sum_{i=1}^{n}\left(\frac{d_{A.i}}{d_{a.i}}\right) > 1 \tag{1}$$

A will decrease in frequency when common (and *a* increase in frequency) if its harmonic mean relative fitness is less than one

$$\frac{1}{\frac{1}{n}\sum_{i=1}^{n}\left(\frac{d_{a.i}}{d_{A.i}}\right)} < 1$$

(2)

Coexistence is assured when these conditions are met because each competitor increases in frequency when rare and decreases in frequency when common.

That both competitors increase in frequency when rare and decrease in frequency when common is a hallmark of frequency-dependent selection(Heino et al., 1998). However, inspecting inequalities 1 and 2 reveals that the ratios of doublings (relative growth rates, relative fitnesses)(Dykhuizen and Dean, 1990; Lenski and Travisano, 1994) are independent of competitor frequencies. Thus, the coexistence predicted by our model is not attributable to frequency dependent selection.

That so simple a model predicts coexistence stands in contrast to much abstract and complex ecological theory, while the prediction of coexistence itself is at variance with classic population genetics (Dempster, 1955).

2.2 Experimental tests

2.2.1 Methods and materials

Media. Rich medium is Luria Broth (LB; 10 g Bacto trytone, 5 g Bacto yeast extract, 10 g NaCl in 1 l ddH_2O) with 15 g/l Bacto agar for solid medium and 8 g/l for soft agar. Minimal medium is Davis salts (MD; 7 g K_2HPO_4, 2 g KH_2PO_4, 1 g $(NH_4)_2SO_4$, and 0.5 g of sodium citrate in 1 l ddH_2O) with 1 ml of 1 M $MgSO_4$•$7H_2O$, 0.5 ml of 1% thiamine, 2 ml of 20% (w/v) glucose stock solution and 1 ml of 50 mg/ml kanamycin (Kan) added after autoclaving. Tetracycline (Tet) and chloramphenicol (Clm) were added at various sub-lethal concentrations as required.

Strain construction. *Tet*^{r} and *Kan*^{r} resistance cassettes were PCR amplified from pBR322 (NEB) and pKD13(Datsenko and Wanner, 2000) and fused together. The paired *Tet*^{r}-*Kan*^{r} cassettes were ligated between 1 kb fragments upstream of *lacI* and downstream of *lacA* (PCR amplified from the *E. coli* MG1655 chromosome) and then ligated into plasmid pRD007 (Poelwijk et al., 2011) using standard molecular cloning procedures(Sambrook, 2001) and propagated in strain DH5α (*fhuA2 Δ(argF-lacZ)U169 phoA glnV44 Φ80 Δ(lacZ)M15 gyrA96 recA1 relA1 endA1 thi-1 hsdR17*). The MG1655 *lac* operon was then replaced by the *Tet*^{r}-*Kan*^{r} construct using the lambda red recombination system(Datsenko and Wanner, 2000). The construct was PCR amplified from the plasmid and transformed into MG1655 cells carrying pKD46 using electroporation (MicroPuler Electroporator, Bio-Rad; 1800 volts, 5.0 milliseconds). Recombinants were selected on LB-Kan plates, screened for Tet resistance (LB plates with 20 μg/ml tetracycline) and the insert confirmed by sequencing. The *Clm*^{r} strain was similarly constructed except *Tet*^{r} was replaced by *Clm*^{r} amplified from pRD007. Note that the derived plasmid was propagated in RecA$^-$ strain DH5α in the presence of kanamycin to prevent loss by deletion.

T5 phage resistant mutants of both strains were isolated by the method of Dykhuizen(Dykhuizen and Dean, 1990). 10^{10} T5 phage (100 μl of lysate) were added to 10^8 cells (100 μl of stationary phase culture grown in LB-Kan) and the mixture added to 4 ml of soft LB-Kan agar (50°C) and plated immediately onto LB-Kan plates. After

overnight incubation at 37°C, T5 resistant colonies were streaked on fresh LB-Kan plates, then grown in liquid LB-Kan and frozen at –80°C in the presence of 15% glycerol.

Competition. T5 sensitive tetracycline resistant (*Tet*^{r}*.T5S*) and T5 resistant chloramphenicol resistant (*Clm*^{r}*.T5R*) strains from – 80 °C stocks were streaked on LB plates supplemented with kanamycin and incubated overnight at 37°C. A single colony from each strain was used to inoculate 1 ml MD media and incubated at 37°C with vigorous shaking (250 rpm) until moderately turbid (OD_{600} between 0.3 - 0.6, 1 cm light path). Strains were mixed in the ratio desired based on OD_{600} readings and used to inoculate a 250 ml sidearm flask with 10 ml MD medium supplemented with a sub-lethal dose of chloramphenicol. Competitions were carried out by incubating flasks at 37 °C with vigorous shaking. Every two hours 200 µl of culture were transferred to a sterile 1.5 ml Eppendorf microcentrifuge tube and stored on ice. At the same time, the population density was determined using a Klett spectrophotometer (with our set up 125 Klett units with a D35 filter (540 nm) is equivalent to 1 OD_{600}, 1 cm light path, or 8×10^8 cells/ml). In competition experiments with fixed carrying capacities population densities above 25 Klett units were monitored frequently and, upon reaching 37.5 Klett units (2.4×10^8 cells/ml), 100 µl of culture inoculated into a second flask of fresh 10 ml MD medium supplemented with a sub-lethal dosage of tetracycline. This transfer procedure was repeated exposing the mixed culture to alternating chloramphenicol and tetracycline with a carrying capacity of 2.4×10^8 cells/ml. The procedures were similar for competition experiments with transfers at fixed 10 hr intervals.

Flow cytometery. The progress of competition was monitored by the T5 method of (Lunzer et al., 2002) with modification. Every 10 hours, ice-kept samples were analyzed in a single batch. To each 200 µl sample were added 42 µl buffer I (equal volumes of fresh LB and T5 lysate (>10^{11} phage/ml) with 5% 20 mg/ml choremphenicol) and 58 µl buffer II (50 µl phosphate buffer (7 g of K_2HPO_4 and 2 g of KH_2PO_4 in 1 liter ddH_2O), 7 µl 62.5 mM Na_2EDTA and 1 µl of 1 mM TO-PRO®-3 (Invitrogen) dissolved in DMSO). The mixture was vortexed and incubated at 37°C for 30 min. After appropriate dilution (to bring the sample density to ~ 10^6 cells/ml) in fresh phosphate buffer cells were counted using a FACSCalibur (BD Sciences) flow cytometer equipped with a 635 nm red diode laser and a 670 nm low pass filter.

The staining procedure allows T5 sensitive and resistant cells to be distinguished. Attachment of T5 phage to sensitive cells depolarizes the cell membranes making them permeable to the TO-PRO®-3 which enters and binds to double stranded nucleic acid. Bound TO-PRO®-3 emits in the far-red (660 nm) upon excitation at 635 nm by a red diode laser. T5 resistant cells remain unstained. Forward scatter and side scatter channels were used together to gate out noise. Typically, data was collected for 50 s (30000 – 75000 events). The density of each strain in the mixed culture was calculated as cell counts/s × dilution factor ÷ flow rate (0.2 µl/s) after correction for background counts.

Experimental Predictions and Data Analysis. The predicted trajectories of the competitions were calculated using Mathematica (version 8.0, Wolfram Research, Inc.). The predictions require nine input parameters: the starting densities of each strain at time

zero, their growth rates in each environment, the carrying capacity, the number of environmental shifts, and the fold dilution at each shift.

New, fitter mutants arising during the competitions would compromise results. Their presence is usually detected between 60 and 80 hours after the start of the competition as a sudden deviation from the predicted growth trajectory. Because we can accurately predict the strain densities far into the future, each competition experiment was initiated at several time points along the expected trajectory, usually at 0, 40 and 80 hrs. These data were then spliced together, with a minimum 20 hrs overlap, to reveal the overall trajectory of the competition.

2.2.2 Results

To test the theory, we conducted competition experiments between two populations of *Escherichia coli*, one resistant to chloramphenicol (Clm^r) and the other resistant to tetracycline (Tet^r). We enforced fluctuating selection by alternating between sub-lethal dosages of each antibiotic in minimal medium with glucose as the sole source of carbon and energy. On reaching an OD_{600} of 0.3 (37.5 Klett units, or approximately $K = 2.5 \times 10^8$ cells/ml), mixed populations were diluted 100 fold into fresh medium containing the alternative antibiotic. This procedure limited population sizes and avoided any physiological complications associated with entering and exiting stationary phase.

Competitions were conducted between a $Clm^r.T5R$ strain resistant to the bacteriophage T5 and a $Tet^r.T5S$ strain that was sensitive to T5. T5 resistance (*fhuA*) serves as a selectively neutral marker that allows the progress of competition to be

monitored by counting individual cells from each population using flow cytometry(Lunzer et al., 2002). This assay is far more rapid and accurate than counting colonies on selective plates.

Table 1 | Predicted and observed relative fitnesses*****

	Pure Cultures			Mixed Cultures		
	Growth Rates μ, h^{-1}**		Predicted Relative Fitness	Growth Rates μ, h^{-1}**		Observed Relative Fitness
Antibiotic	*Clm^r.T5R*	*Tet^r.T5S*	$w_{Tet^r.T5S}^{Clm^r.T5R}$	*Clm^r.T5R*	*Tet^r.T5S*	$w_{Tet^r.T5S}^{Clm^r.T5R}$
Chloramphenicol	0.62	0.28	2.21	0.64	0.29	2.21
Tetracycline	0.30	0.59	0.51	0.30	0.59	0.51
Arithmetic Mean			1.36			1.36
Harmonic Mean			0.83			0.83
Geometric Mean			1.06			1.06

*Antibiotic concentrations: 0.12 μg/ml chloramphenicol and 0.55 μg/ml tetracycline.

**Standard errors are less than 1.5% of all estimates.

Pure cultures growing at sub-lethal antibiotic concentrations of 0.12 μg/ml chloramphenicol and 55 μg/ml tetracycline predict an arithmetic mean relative fitness greater than one and a harmonic mean relative fitness less than one – conditions sufficient for coexistence (**Tab. 1**). As predicted, populations competing in mixed culture under

these conditions converge on a stable oscillatory coexistence regardless of their initial frequencies (**Fig. 1a**). Changing the antibiotic concentrations shifts the equilibrium midpoint of the oscillations up and down (**Fig. 1b**). This shows that coexistence is robust to perturbations. The selection is not frequency-dependent – growth rates remain constant regardless of population frequencies and densities (**Fig. 2**).

We can recover the behavior predicted by classic population genetic theory if, instead of transferring the mixed culture at a predetermined population size, we transfer it after a fixed period of time. The *Clm*^{r}*.T5R* population has the larger geometric mean fitness and is now predicted to win the competition (**Tab. 1**). Under precisely the same environmental conditions that led to coexistence in FIG. 1a, but now with transfers every t = 10 hrs regardless of population density, the *Clm*^{r}*.T5R* population is destined for fixation (**Fig. 1c**). And under precisely the same environmental conditions that led to coexistence in **Fig. 1b** (dots), the *Clm*^{r}*.T5R* population is now destined for extinction (**Fig. 1d**) with transfers every t = 10 hrs. Coexistence and competitive exclusion depend on the transfer regime.

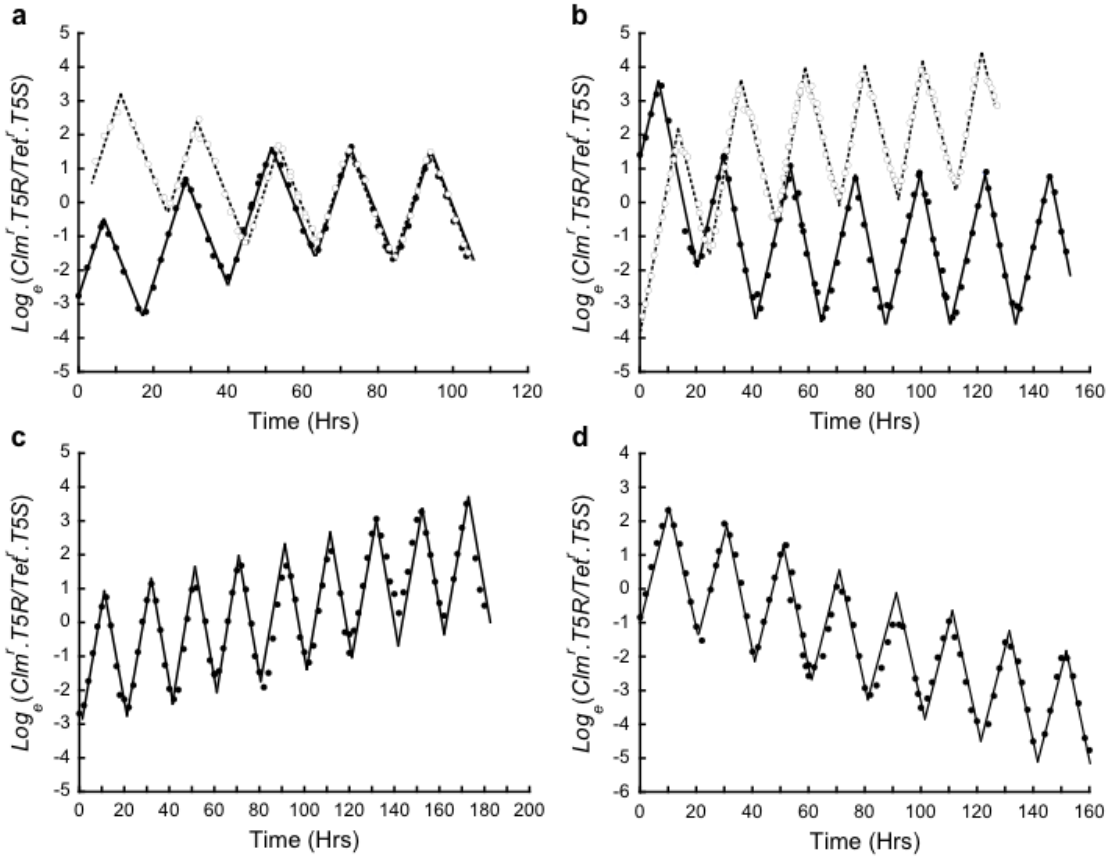

Figure 1| The outcome of competition with alternating directional selection depends on the mechanism of population regulation. **a** and **b**, Competing clones coexist in cultures regulated in density dependent manner. **a**, Two mixed cultures (circles and dots), initiated at different clone frequencies, converge rapidly onto the same stable oscillation (alternating 0.12 µg/ml chloramphenicol and 0.55 µg/ml tetracycline). On reaching a density of 2.4×10^8 cells/ml cultures were immediately diluted 1/100 into fresh medium containing the alternate antibiotic. **b**, Changing the concentrations of the antibiotics changes the selection intensities and shifts the stable oscillation up (circles, chloramphenicol now 0.22 µg/ml) and down (dots, tetracycline now 65 µg/ml). **c** and **d**, Competing clones cannot coexist in cultures regulated in a density independent manner. Transferring cultures to fresh medium every 10 hours regardless of population density leads to competitive exclusion (**c**, antibiotic concentrations identical to **a**; **d**, antibiotic concentrations identical to **b**-dots). The selection coefficients per hour (slopes) depend only on antibiotic concentrations and remain invariant regardless of clone frequencies, culture densities, and mechanisms of population regulation.

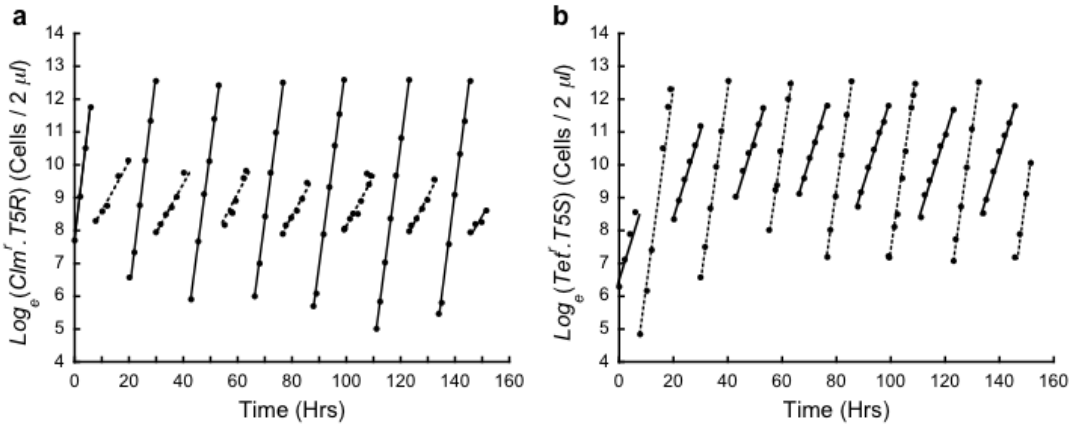

Figure 2 | Growth rates are fixed. Growth rates of the clones (**a**, Clmr.T5R and **b**, Tetr.T5S) remain invariant at 0.12 μg/ml chloramphenicol (lines) and 0.65 μg/ml tetracycline (dashes) demonstrating that growth rates are neither frequency nor density dependent. Data from **Fig.1b**-dots.

2.3 Discussion, simulation and conclusion

2.3.1 Carrying capacities are critical to coexistence

To understand the role of carrying capacities in promoting coexistence we have only to consider a serial transfer experiment in which a mixed culture is diluted, say 1024-fold, and grown to full density. If competitor a is common and a fitter competitor A ($\mu_A/\mu_a = d_A/d_a > 1$) is rare, then it follows that the number of doublings by a is $\log_2 1024 = 10$, and that the number of doublings by A is $10 \cdot d_A/d_a > 10$. However, if A is common and a is rare then it follows that the number of doublings by A is 10, and that the number of doublings by a is $10 \cdot d_a/d_A < 10$. In resource-limited environments competitors experience more doublings when the least fit competitor is most common. It's not relative fitness that's frequency-dependent; it's the number of generations (i.e. the number of doublings) per dilution that's frequency-dependent.

Now suppose the fitness of *A* relative to *a* is 2 in environment 1 and 0.5 in environment 2. When common, *a* experiences 10 doublings in each environment following dilution and growth to carrying capacity, while the rare *A* experiences 20 doublings in environment 1 (where it's twice as fit) and 5 doublings in environment 2 (where it's only half as fit). For every cycle of two environments *a* experiences 20 doublings whereas *A* experiences 25 doublings. The argument is symmetrical with respect to *A* and *a*; when *A* is common it experiences 20 doublings while the rare *a* experiences 25 doublings (**Tab. 2**). Hence, each competitor invades when rare because it experiences more doublings than its common rival which remains strictly resource limited. The result is something akin to the storage effect in ecology(Chesson, 1983) where the advantage to rare competitors of reproduction in good environments exceeds the cost of reproduction in poor environments. External limits to population size passively bias competition in favor of rare competitors, and in so doing promote coexistence.

Table 2| Doublings in a fluctuating environment*

		Doublings		
		Environment		
Competitor	Frequency	1	2	Sum
A	rare	20	5	25
a	common	10	10	20
A	common	10	10	20
a	rare	5	20	25

* Fitness of *A* relative to *a* ($\mu_A/\mu_a = d_A/d_a$) is 2 in environment 1 and 0.5 in environment 2 in this hypothetical serial transfer experiment with 2^{10}-fold dilutions.

With fixed time periods, as in classic population genetics, the doublings in each environment by each competitor are fixed. A rare competitor *A* invading a population *a*, whose doublings precisely match the 2^{10}-fold dilution at each transfer, must grow to infinity since $2^{d_{A.1}+d_{A.2}}/2^{20} > 2^{d_{a.1}+d_{a.2}}/2^{20} = 1$. The assumption that resources are infinite was introduced to population genetics when it was supposed that continuous time overlapping generation population growth could be accurately represented by a discrete generation time model with normalized growth rates (i.e. relative fitnesses). Far from describing competition, the population genetic model instead describes ecological neutralism, for without limiting resources there is no competition, no struggle for existence. The clones do not interact. They simply reproduce and die.

2.3.2 Simulation with general case

The case at focus so far is only minimal and special: two competitors and two regularly alternating environments. Now, consider two competitors in a series of environments, where the growth rates for each competitor is randomly drawn from a distribution. The probability that they coexist in two environments is 0.193 when growth rates are chosen a uniform distribution. The probability of coexistence increases with more environments and decreases with the number of species that must coexist (**Fig. 3a**). Trade-offs in fitness increase the likelihood of coexistence (**Fig. 3b**). The probability that two competitors coexist in two environments is 0.5 with a linear trade-off. The impact can be dramatic – coexistence is guaranteed for two species in two environments when the fitness trade-off

has the form $w_1 = 1/w_2$. We assert that temporal variability in competition is as important as spatial variability in promoting biological diversity.

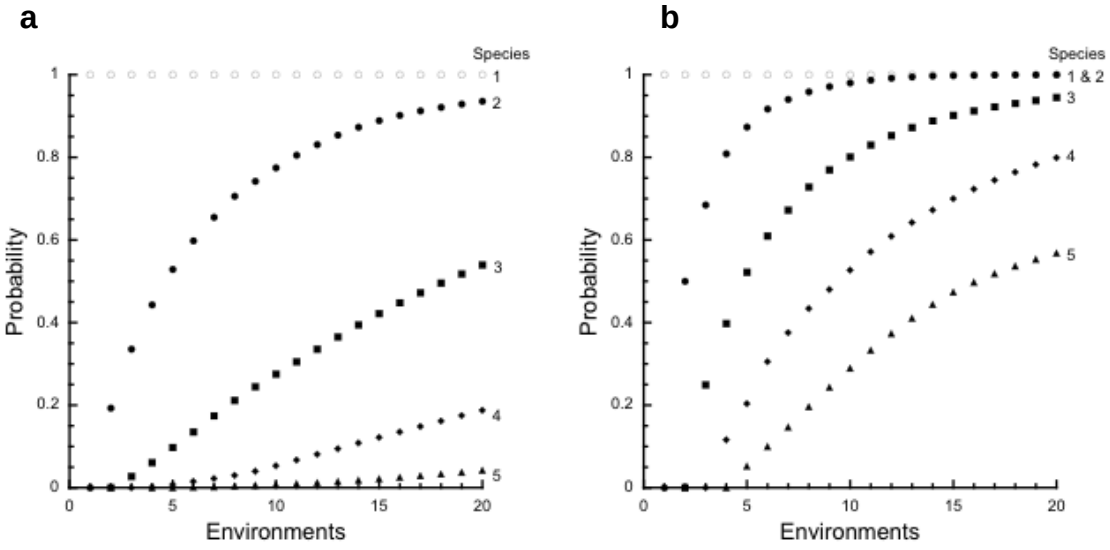

Figure 3 | Probability of coexistence in variable environments. **a**, The probability of coexistence increases with the number of environments but decreases rapidly with the number of species in the absence of fitness trade-offs. Growth rates for each species in each environment were drawn randomly from a uniform distribution. **b**, Coexistence is much more likely in the presence of fitness trade-offs. Summing and normalizing the growth rates of each species introduces fitness trade-offs.

Now consider a general situation where new competitors, i.e., genotypes, are introduced to the population by mutations and old ones die out due to random sampling for death. Then we can study how fluctuating environments affect the diversity of competitors in the population. Moran model accommodates such situation: evolution carries on in discrete time steps; each step, one individual is randomly chosen for death and one competitor (genotype) is chosen to increase its number of individuals by one according to the growth rate—competitors with higher growth rate is more likely to be

chosen; with a small probability of occurrence, a random individual is mutated to a novel genotype assuming a infinite pool of genotypes; then go to the next step and repeat. Since population is always kept at its full size, this model fulfills the fixed carrying capacity condition from the minimal model.

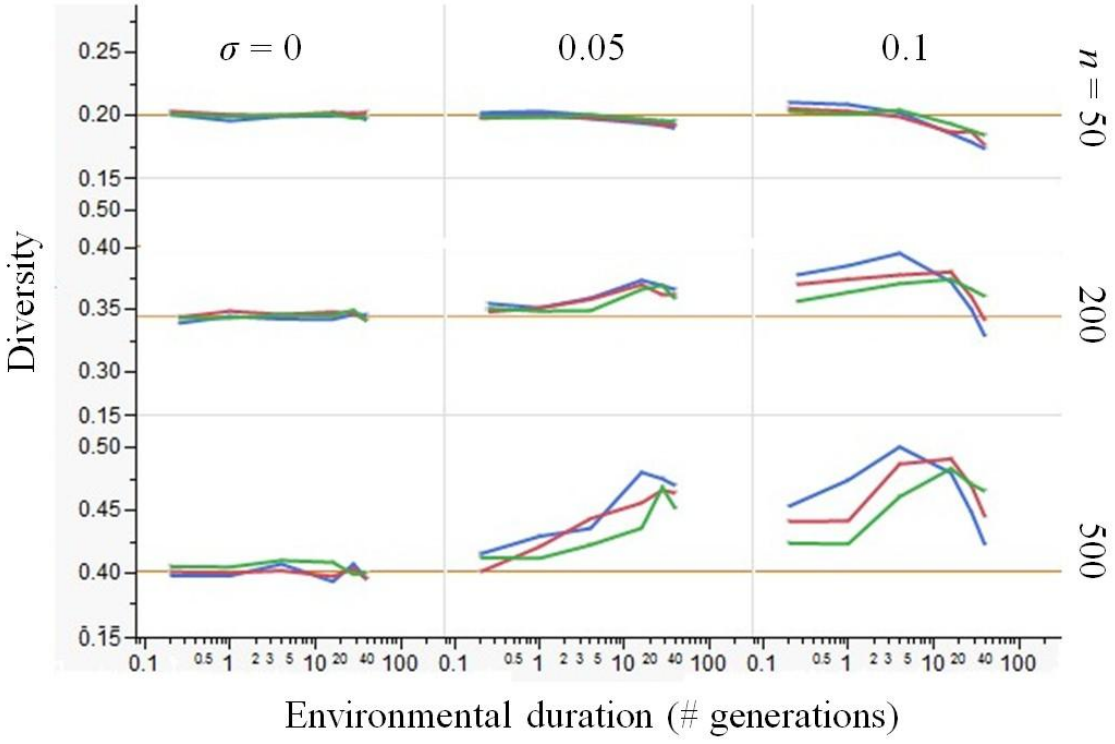

Figure 4 | Diversity as a function of environmental durations (reciprocal of shifting rate), population size (n), standard deviation of growth rates distribution (σ) and correlation among competitors in their response to environmental change. Diversity is defined by Simpson's index: $1-\sum N_i(N_i-1)/(N(N-1)$, where N_i is the number of individuals for competitor of genotype i and N is the total number of individuals in the population. Growth rate distribution is log-normal with mean of one, varying standard deviation (σ) and varying correlation coefficients between competitors: 0 (blue), 0.3 (red), 0.6 (green). Generation time is the same as population size because one individual dies at each step and the population turnover time is the number of individuals in the population. Mutation rate is 0.005. Each data point is the average of 3000 realizations of simulation, each summed from a time series with the number of time steps four to 20 generations. The orange lines are the baseline of diversity set by pure drift without fluctuating selection.

Surprisingly, fluctuating environments ($\sigma \neq 0$) boosts diversity of competitors in a wide area of parameter space (**Fig. 4**). Two exceptions are: when population size are as small as 50 individuals, genetic drift is dominant and environmental fluctuation reduces diversity when strong ($\sigma = 0.1$) ; or when environmental duration is long (> 30 times generation time), i.e., infrequent shifting, selection purges divsersity. Interestingly, maximum diversity occurs at an intermediate level of environmental duration (between four to 30 times generation time). Worth noting, adding correlation among competitors in their growth response to environmental change does not neutralize the boost effect: correlation coefficient of 0.6 shows the same trend as no correlation.

2.3.3 Synthesis

Temporal variability has been considered either unimportant (Schoener, 1974; Turelli and Gillespie, 1980) or detrimental (May, 1973) to promoting coexistence because the necessary conditions were thought to be either too restrictive or impossible to meet(Dempster, 1955; Felsenstein, 1976; Gillespie, 1972; Haldane and Jayakar, 1963; Hartl and Cook, 1974; Karlin and Liberman, 1975; Kimura, 1954). Recent theoretical and field observations (Cáceres, 1997; Chesson, 2000; Dean, 2005; Pake and Venable, 1996) challenge this view, suggesting instead that temporal variability might play a major role in maintaining diversity. Our experiments demonstrate that temporal fluctuations in selection are sufficient to promote coexistence during competition for a single limiting resource. Fitness need not be frequency-dependent.

Inequalities 1 and 2 for coexistence in a temporally variable environment are identical to those for coexistence in a spatial model of competing clones that disperse

randomly into habitats at each generation (Gliddon and Strobeck, 1975). In a randomly mating diploid population coexistence of two alleles is ensured when the harmonic mean fitnesses of both homozygotes, with respect to the heterozygote, are less than one. This condition, which prevents fixation of either allele, is identical to Levene's (Levene, 1953) spatial model of selection with random dispersal of zygotes to different habitats each generation. We conclude that, absent restrictions to migration among habitats, temporal and spatial environmental variability have similar capacities to maintain genetic diversity. Moreover, the generalized model by simulation provides an alternative to the neutral theory (Kimura, 1983), standard explanation of the rich genetic polymorphism observed from nature. Opposite to its genetic drift-centered view, the model presented here suggests that differential response to fluctuating selection can maintain high level of polymorphism—competition counter-intuitively facilitates diversity and can even do better than drift!

Competition among species is equivalent to competition among asexual clones - in both cases reproductively isolated populations compete for limiting resources. Despite sharing this commonality, theoretical ecology and population genetics have taken dissimilar approaches to assessing the impact of competition on biological diversity. Ecological models describe population growth rates in terms of resource abundances, population densities and interactions between species. Population genetic models treat relative fitnesses as independent variables and not as the emergent properties of underlying ecological and organismal processes. Our theory provides a conceptual

oundation that unifies these two fields, and at the same time strikes a balance between realism and clarity.

Chapter 3

Adaptation in fluctuating environments

More than deviate from the constant and homogenous environments in laboratory, nature constitutes a whole different world. In particular, the dynamic and intrinsically stochastic fluctuations in critical conditions for life command serious survival strategies. Signal that predicts or, less stringently, correlates with certain environmental change can be sensed by organisms, which then make decisions accordingly as to how to respond. This has become the most familiar form of behavior to modern biological sciences, with virtually all examples of regulated gene expression falling into this category. In the example of the classic *lac* operon in *E. coli*, the presence of lactose inactivates the repressor, leading to the expression of genes that are required for the metabolism of the sugar (Jacob and Monod, 1961a).

In the above example, the signal is 100% reliable because the signal molecule itself is the environmental change that the bacteria need to deal with, i.e. catabolizing for energy. However, there are other occasions where the signal is multiple steps away from the actual environmental change such as in signaling transduction. The signal thus becomes vulnerable to lag, noise or distortion arising from the intermediate steps of information cascade, all of which undermine its reliability (Kaern et al., 2005; Tan et al., 2007). Now, an alternative strategy, bet-hedging, might be advantageous. An isogenic population of organisms develop into phenotypically heterogeneous subpopulations. Their immediate fitness might be suboptimal due to the mismatch of certain subpopulation to the current environmental state, whereas the long term survival of the

overall population across multiple environmental fluctuations are buffered from collapse (Simons, 2009).

As studies of gene regulation provide numerous examples of sensing strategies that are intensively studied at the molecular level (Hurme and Rhen, 1998; Jacob and Monod, 1961b), bet-hedging has remained elusive to mechanistic elucidation until the emergence of research interest in noise since the recent decade. Stochastic gene expression becomes under close examination with advanced theories and experimental techniques (Eldar and Elowitz, 2010). Many biochemical reactions within cells involve only small numbers of molecules. For example, no more than five copies of mRNA are present for a typical gene expressed in an *E. coli* cell (Taniguchi et al., 2010). Probabilistic encounters between small numbers of molecules render many reactions stochastic (Shahrezaei and Swain, 2008). For example, stochastic gene expression in *Bacillus subtilis* underlies the phenotypic heterogeneity where only a small fraction of cells sporulate, a costly process that may confer a large fitness advantage under adverse conditions (Veening et al., 2008). Therefore, stochastic gene expression provides a plausible mechanism for bet-hedging. Despite mounting scenarios as abovementioned, rigorous test is still lacking.

This chapter aspires to develop and test a model of bet-hedging. It will be shown that the standard prediction of bet-hedging fails at biologically relevant scenarios and that bet-hedging is an extremely advantageous strategy in changing environments.

3.1 Model

The central theme of this project is bet-hedging strategy and its relationship to responsive sensing in the context of evolution. The standard bet-hedging theory will first be introduced, followed by description of a model based on stochastic phenotype switching. This model will be numerically analyzed, and critical predictions will be made for experimental tests in the next section. Most noticeably, the current model based on extensive simulation identifies a biologically relevant region in the parameters space that defies the classic prediction from standard bet-hedging theory—optimal phenotypic switching rate shall mimic environmental shifting rate.

3.1.1 Bet-hedging theory

From the evolutionary perspective the quantity that needs to be maximized is long-term mean fitness—even if immediate fitness under the prevalent environmental conditions is suboptimal. For a clonal species, this quantity is written as

$$\omega = e^{\sum_{i=1}^{n} r_i t_i / \sum_{i=1}^{n} t_i} \tag{3}$$

where ω is the intergenerational geometric mean fitness, and r_i and t_i are the growth rate and the time spent in the i^{th} of n environments (Gillespie, 1972). The relative fitness of competitor 1 and competitor 2 is $\omega_2^1 = \omega_1 / \omega_2$. In a changing environment, sensing strategies might not be optimal due to the unreliability of the signal and the swiftness of the environmental changes. In this situation, ω will be reduced because of the large variance in growth rates of individual generations (r_i). Theory (Kussell and Leibler, 2005) predicts, in bet-hedging strategies, as the switching frequencies between multiple states

mimics the changing frequencies of the environment, the geometric mean fitness ω gets maximized.

3.1.2 Model of stochastic switching

Consider a strain with two phenotypic states (expressing or non-expressing a fitness-determining gene) inhabiting either of two environments. The following formula describes the time evolution of the population:

$$\frac{d\vec{N}}{dt} = G_{\varepsilon(t)}\vec{N} \qquad \text{where } \vec{N} = \begin{pmatrix} n_1 \\ n_2 \end{pmatrix} \text{ and } G_k = \begin{bmatrix} r_1^{(k)} - s_{12}^{(k)} & s_{21}^{(k)} \\ s_{12}^{(k)} & r_2^{(k)} - s_{21}^{(k)} \end{bmatrix} \tag{4}$$

where the vector $\vec{N}$ consists of the densities of the two subpopulations of the strain: n_1 (expressing) and n_2 (non-expressing). The matrix G_k governs the growth rates of the subpopulations. k denotes the environmental states ($k = \alpha, \beta$), r's are the intrinsic growth rates and s' are the switching rates with the subscripts indicating the direction of switching (e.g. subscript 12 indicates a switch from expressing to non-expressing and vice versa). $\varepsilon(t)$ is a function that specifies the occurrence of switching from one environmental state to the other. This model readily describes the bet-hedging strategy. To accommodate sensing strategies, the assignments of values of r's should be determined by a cue that is in turn correlated with the environmental shifts and s' should be zero. With numerical algorithms, the geometric mean fitness ω, relative fitness ω_2^1 can be computed precisely. Importantly, this model allows relative fitness in mixed competition to be predicted from the growths of pure strains in isolation.

3.1.3 Long term fitness in cyclic environments

Re-arrangement of equation (4) leads to the following:

$$\frac{dp}{dt} = -ap^2 + (a-b)p + c \tag{5}$$

where p is the fraction of expressing subpopulation, $n_1/(n_1+n_2)$; a is the growth rate difference between the expressing and non-expressing subpopulations, r_1-r_2; b is the sum of the two switching rates, $s_{12} + s_{21}$; and c is s_{21}. Analytical solution to this equation has the form:

$$p = \frac{1}{2a}(a-b+l\frac{1-Ae^{-lt}}{1+Ae^{-lt}}) \tag{6}$$

where l is $\sqrt{(a+b)^2+4ac}$ and A is a constant determined by boundary condition. Now, let's assume the environments α and β are symmetrical in that each has duration $T/2$ and the growth rate difference between the expression and non-expressing subpopulations are the same but with flipped sign, i.e. the advantage of expressing the gene is reversed going from one environmental state to the other.

Assume the environment regularly alternates between two states (α, β). The dynamic system of equation (4) is expected to stabilize into repetition of a defined period. We can calculate the exact form of p in a full cycle of the alternating environment:

$$p(t) = \begin{cases} p_\alpha(t) = \frac{1}{2a}(a-b+l\frac{1-Ae^{-lt}}{1+Ae^{-lt}}) & 0 \le t < T/2 \\ p_\beta(t) = \frac{1}{2a}(a+b-m\frac{1-Be^{-m(t-T/2)}}{1+Be^{-m(t-T/2)}}) & T/2 \le t < T \end{cases} \tag{7}$$

where m is $\sqrt{(-a+b)^2-4ac}$, B is a constant determined by boundary condition and

environmental states α, β correspond to the time periods [0, T/2) and [T/2, T) respectively. After stabilization, $p_\alpha(0) = p_\beta(T)$ and $p_\alpha(T/2) = p_\beta(T/2)$. These two boundary conditions allow determination of the values for A and B, rendering $p(t)$ readily solvable numerically. Analytical solution is possible(Gerland and Hwa, 2009), but requires the assumption that the time scale of stabilization of the system when a new environmental state arrives is much shorter than the duration of the state. This assumption would exclude analysis of a large domain where the environmental fluctuations are rapid, e.g. not much slower than the organisms' generation time. In order to calculate overall growth rate in the fluctuating environment, integration of $p(t)$ over T is taken:

$$w_P^S = \frac{2}{T(r_1 + r_2)} \int_0^T \{r_1^{(k)} p(t) + r_2^{(k)}[1 - p(t)]\} dt \tag{8}$$

Now, consider responsive sensing. First, signal that is not lagged but unreliable. In other words, cellular, i.e. growth rate, response is immediately completed upon sensing of the signal but there is the chance of 1- γ that the signal indicates wrong environmental state. We have the overall growth:

$$w = \frac{1}{T}\{\int_0^{T/2} [r_1^{(\alpha)}\gamma + r_2^{(\alpha)}(1-\gamma)]dt + \int_{T/2}^{T} [r_2^{(\beta)}\gamma + r_1^{(\beta)}(1-\gamma)]dt\} \tag{9}$$

Next, signal that is lagged but reliable. Assume the population starts as 100% non-expressing and enters environment α, and starts to gradually express the gene so that the growth rate change follows a Monod-like dynamics:

$$p_\alpha(t) = p(0)e^{r_\alpha(t)} \tag{10}$$

where $r_\alpha(t) = r_2 + \frac{r_1 t}{\tau + t}$ with τ being the time to achieve the middle point between the

initial and maximum growth rates. As the underlying mechanism is induction of gene expression, τ is determined by the kinetic properties of the gene expression machinery. When the environment β arrives, signal for α as well as induction of gene expression disappears, and the time evolution of the population becomes:

$$p_\beta(t) = p(T/2)e^{r_\beta(t-T/2)} \tag{11}$$

where $r_\beta(t) = r_1 + \frac{r_2 t}{\eta + t}$ with η being the time to the middle point between the initial and maximum growth rates. Here, the underlying mechanism is protein degradation and dilution due to cell division. The overall growth rate of the responsive sensor then becomes:

$$w = \frac{1}{T}[\int_0^{T/2} r_\alpha(t)dt + \int_{T/2}^{T} r_\beta(t)dt] \tag{12}$$

Lastly, consider two easy scenarios: constitutive expression and permanent silence (non-expressing), i.e. passive observer of the environment. Their respective overall growth rates are given by:

$$w = \frac{1}{2}(r_1^{(\alpha)} + r_1^{(\beta)}) \tag{13}$$

$$w = \frac{1}{2}(r_2^{(\alpha)} + r_2^{(\beta)}) \tag{14}$$

Equations (8), (9), (12), (13) and (14) establish a platform for systematic comparison between different strategies under varying conditions and constitute a generator of predictions for downstream experimental tests.

3.1.4 Model simulations and predictions

Basic model of bet-hedging. Bet-hedging sits as the central piece, so the initial analysis is done to survey its basic properties. The primary interest on bet-hedging is the fitness advantage it brings about. To put it in an evolutionary context, it is natural to quantify this advantage by calculating the relative fitness of bet-hedger over non-hedger(Lenski), i.e. the ratio of equation (8) over equation (13). Here, further simplifying treatment of the model is made: the growth rates are symmetrical between the two environments and switching rates between the two phenotypic states are the same as shown in **Tab. 3**. By doing so equations (13) and (14) become equivalent.

Table 3 | Model setup*

Phenotype	Switching away rate	Growth rate		Duration	
		Environment		Environment	
		α	β	α	β
Expressing	s	r_1	r_2	T	T
Non-expressing	s	r_2	r_1		

***** $r_1 > r_2$ and shifting rate of the environment is $1/T$.

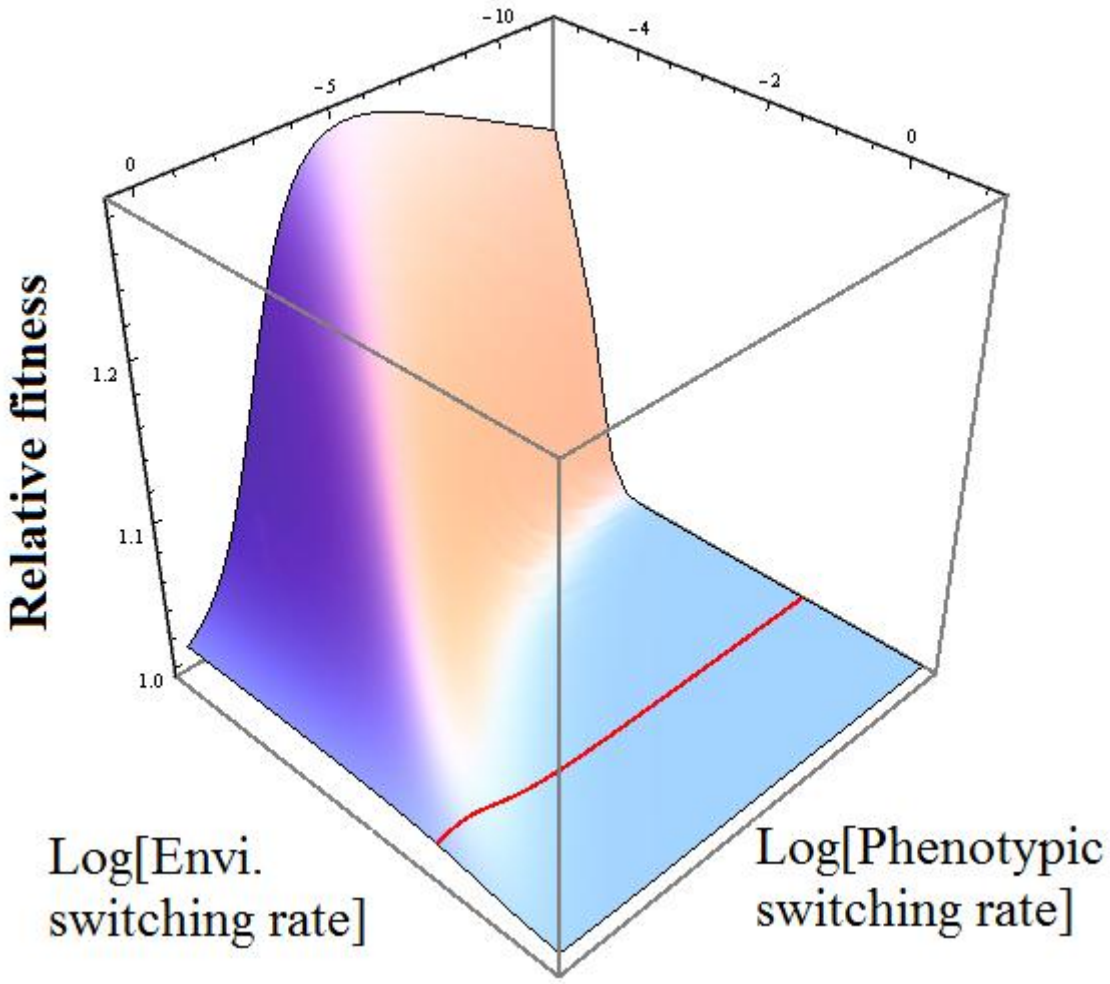

Figure 5| Relative fitness of bet-hedger over non-bet-hedger (passive observer). $r_1 = 0.6$ generations per hour and $r_2 = 0.3$ generations per hour. Units for environmental and phenotypic switching rates are on par with that of the growth rates. Relative fitness is the ratio of overall growth rates for bet-hedger over passive observer. The red curve indicates a changing rate of 0.45, which is the overall growth rate for the passive observer.

With a fixed pair of r_1 and r_2, we can ask how phenotypic switching rate and environmental switching rate interact to determine the relative fitness of bet-hedger over passive observer. From **Fig. 5**, it becomes obviously that bet-hedging is widely advantageous. In environments that are rapidly shifting, i.e. the region beyond the red curve in the figure, environmental durations are shorter than the generation time of organisms, and the landscape topology is almost flat with the relative fitness close to one. To the contrary, when the environmental fluctuation slows down, the advantage of phenotypic switching increases dramatically in two ways.

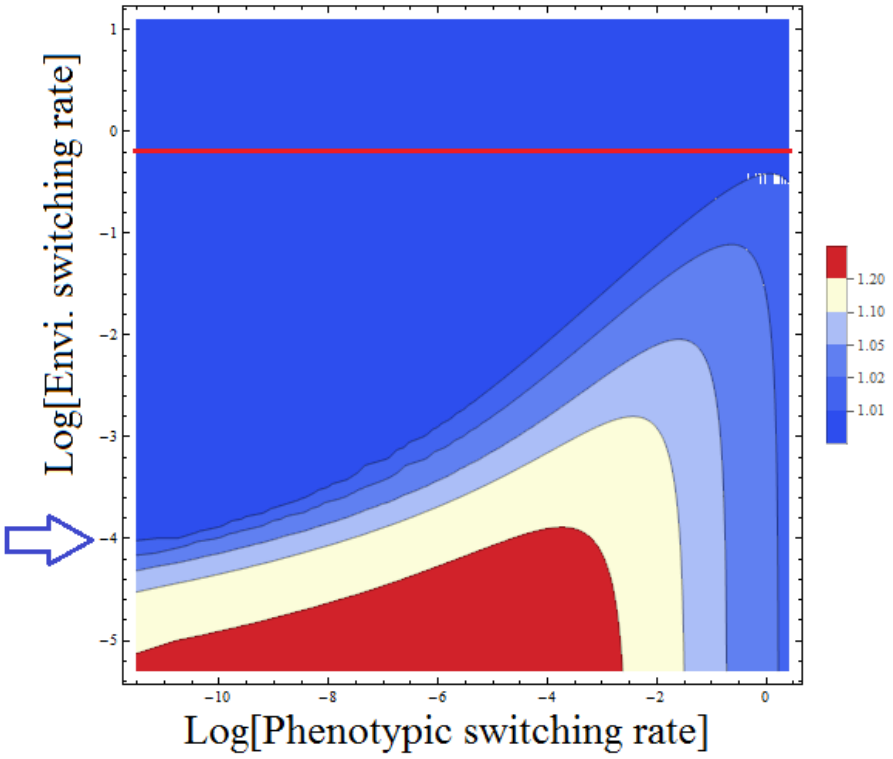

Figure 6 | Relative fitness contour plot. The data is the same as in **Fig. 5**. The arrow indicates environmental shift rate of 0.018. The red mesh curve indicates a changing rate of 0.45, which is the overall growth rate for the passive observer. The legend denotes the relative fitness levels.

First, the range of beneficial phenotypic switching becomes broader at lower environmental shifting rates. As shown from **Fig. 6**, when the environment fluctuates at the rate of 0.018 or lower, all phenotypic switching rates simulated here, ranging from 0.00001 to 1.5, bring about relative fitness of at least 1.01. That is 1% growth advantage per unit of time (hours in here), making a significant selective advantage. Second, The maximum relative fitness for each environment increases as the environmental shifting rate decreases (**Fig. 7**) before saturating at exceedingly low rate of environmental shift. To my knowledge, this significant relationship between evolutionary advantage of bet-hedging and rate of environmental shifts has not been explored before.

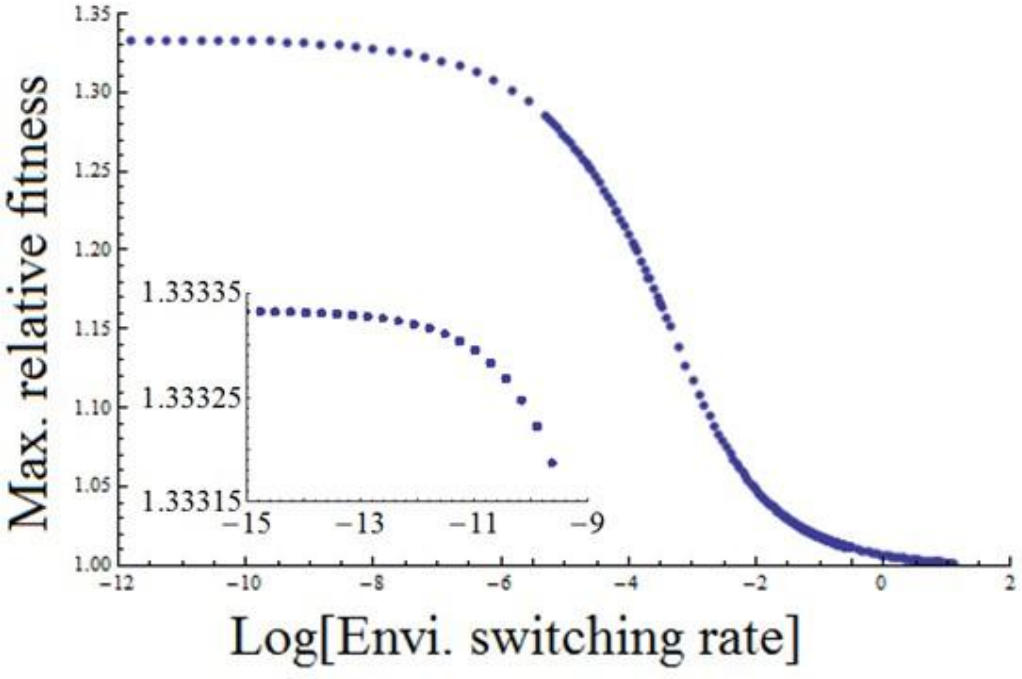

Figure 7 | Maximum relative fitness of bet-hedger increases in infrequently shifting environments. The conditions are par with those in **Fig. 5**. The inset zooms in at the region of extremely low environmental shifting.

To find an analytical explanation, go back to equations (7) and (8) that govern the overall growth rate for bet-hedger. Because the overall growth rate of passive observer is time-independent, we need not to take the denominator of relative fitness into account. In the region of infrequent environmental shifting (but not extremely low end), also whereby high relative fitnesses occur, the duration within each environment is much longer than the time it takes for the phenotypic switching to equilibrate. Mathematically, after rearrangement, equation (7) can be re-written as:

$$p_\alpha(t) = \frac{1}{2a}\{a+b-l\tanh[\frac{l}{2}(t-\log(A)]\} \approx \frac{1}{2a}(a+b-l) \tag{15}$$

Hyperbolic tangent (tanh) is an asymptotic function. When *t* is allowed to proceed for long enough, the initial phase of equilibration can be neglected, i.e. treating tanh(*x*) as 1, leading to the approximation made in equation (15). The same operation can be done to $p_\beta(t)$. Plug into equation (8), yielding the following expression:

$$w = \frac{(m+l-2b)+2(r_1+r_2)}{4} = \frac{(\sqrt{a^2+4c^2}-2c)+(r_1+r_2)}{2} \tag{16}$$

Take derivative of *w* with respective to *c*,

$$\frac{dw}{dc} = \frac{4c}{\sqrt{a^2+4c^2}} - 2 = 2(\frac{1}{\sqrt{\left(\frac{a}{2c}\right)^2+1}} - 1) \leq 0 \tag{17}$$

where it is obvious that the inequality always holds. Therefore, *w* is a decreasing function of *c*. This analysis focuses on the benefit of bet-hedging at extreme cases where initial dynamics can be ignored, it turns out, under this condition, switching seems to incur cost: if we make *c* equals 0, *w* becomes the highest possible in the current environmental

configuration. Of course, this is problematic. The reason for this problem is that this analysis assumes swift transition of the population from the previous environment to the optimal composition at the current environment. Effectively, it ignores the cost associated with the suboptimal population composition during the equilibrating phase and emphasizes the cost of switching from the favored to the unfavored phenotypes at the equilibrated late stage. It at the best explains the trend at the very low rate of environmental shifting (**Fig. 7**, inset). By examining a series of time evolution for $p(t)$ with optimal fitness, a more important factor in determining the pattern is identified. As shown in **Fig. 8**, it is the exact initial phase of dynamic equilibration that underlies the difference in the relative fitness benefits. Starting from fast shifting environments (**Fig. 8**, lower right), the equilibration phase spans the whole environmental duration and never reaches the equilibrated state. As the rate of environmental shifting rate decreases, equilibrium of the population composition becomes reached and the fraction of time spent in the initial equilibration phase decreases. Then, a question strikes immediately: could the relatively low fitness at high rates of environmental shift be improved by further increasing the phenotypic switching rate? The answer is no. Too rapid switching should undo the beneficial enrichment of the favorable phenotype in the population. **Fig. 9** demonstrates this adverse effect of hyper switching. As the switching rate increases, the equilibrated state indeed becomes reachable, evidenced by the flat segment of the curves. But the equilibrium fraction of the favored phenotype is substantially reduced, leading to the drop of fitness. In conclusion, the negative relationship between the optimal relative fitness and the shifting rate of the environment (**Fig. 7**) at

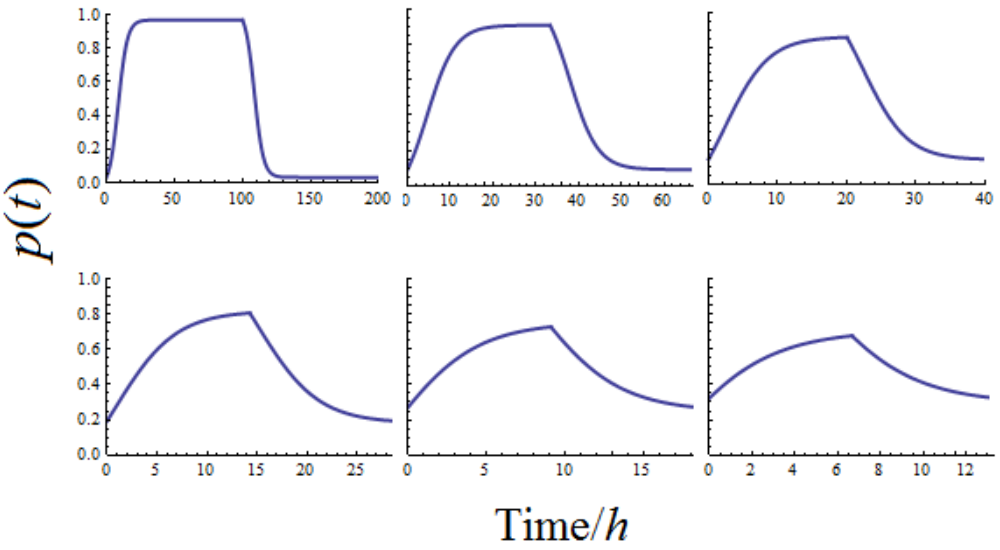

Figure 8 | Time evolution of the fraction of the expressing phenotype in the population. r_1 = 0.6 generations per hour and r_2 = 0.3 generations per hour. For each panel, the switching rate is the one giving maximum relative fitness from simulation. Starting from top left to lower right panels, the environmental shifting rates are 0.01, 0.03, 0.05, 0.07, 0.11, 0.15.

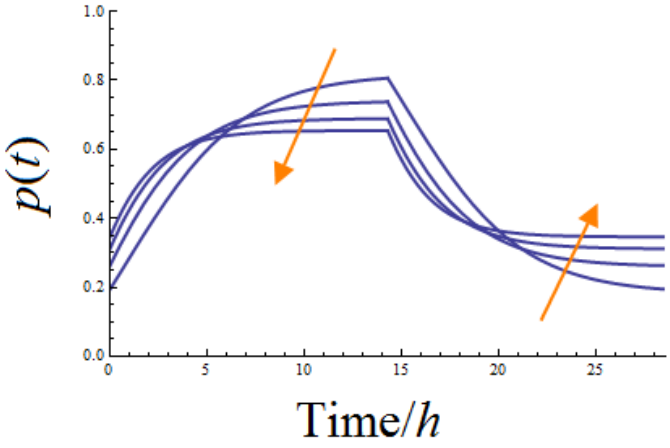

Figure 9 | Effect of hyper switching on $p(t)$. The conditions are par with those in **Fig. 8**. The environmental shifting rate is fixed across all curves to be 0.07. The orange arrows indicate the increasing trend of switching rates starting from 0.07 to 0.12, 0.17 and 022.

intermediate range of shifting rate of the environment is due to the fact that the mixed population spends a larger fraction of the entire environmental duration in the equilibrated state as the environmental shifting rate decreases. On the other hand, rapidly changing environments limit fitness benefit that bet-hedging brings about by enforcing extension of the equilibrating phase.

Global behavior of the bet-hedging model. Three type of rates determine the advantage of bet-hedging: phenotypic switching rates, environmental shifting rates and growth rates. In the previous section, the first two have been discussed. Now, let us consider growth rates. **Fig. 10** shows the maximum relative fitness as environmental shifting rates and growth rate ratio r_2/r_1 vary (r_1 is fixed). First note that increasing and saturation of bet-hedging advantage respectively at intermediate and low environmental shifting rates are a global feature across all growth rate ratios. Second, high advantage of bet-hedging is achieved at low environmental shifting rate and low r_2/r_1, i.e. large growth differentials between environments. As the growth rate ratio decreases, maximum relative fitness accelerates. The unique feature of the current model is its focus on the transitioning/equilibrating phase initiated at the arrival of a new environment. The consequence is the discovery of a non-trivial range of environmental shifting rates where the system's behavior deviates from the standard theory. The standard theory predicts that optimal phenotypic switching rates should be fine-tuned exactly to the environmental shifting rate (Kussell and Leibler, 2005; Simons, 2009). However, optimal phenotypic switching rates systematically diverge from the prediction at intermediate and high environmental shifting rates (**Fig.**

11). The extent of deviation is bounded at 60%, i.e., the optimal phenotypic switching rates are 60% faster than predicted by the standard theory.

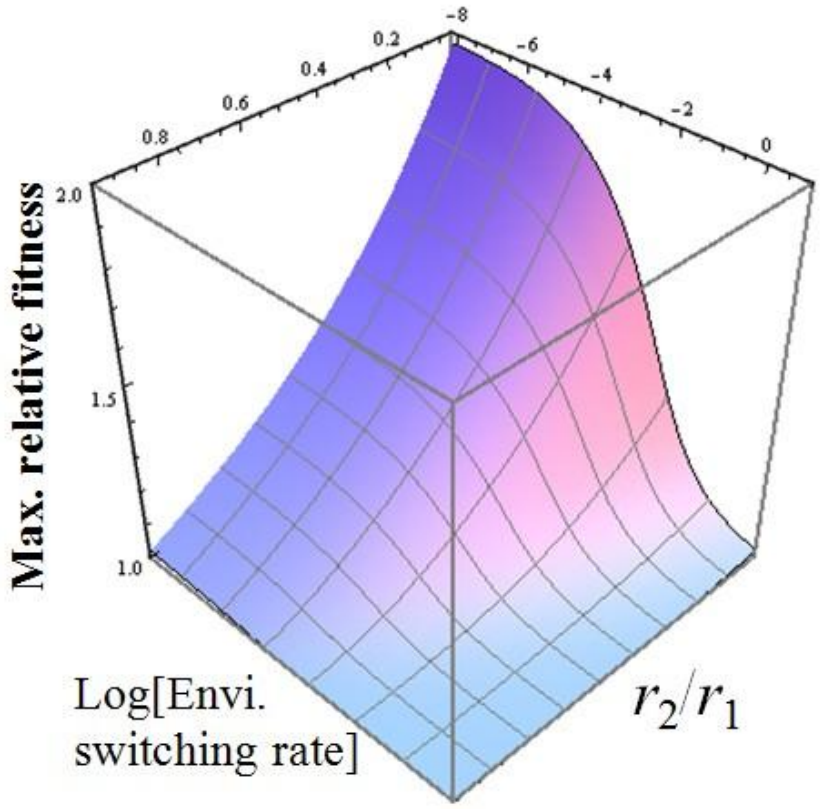

Figure 10 | Maximum relative fitness as a function of environmental shifting rate and the growth rate ratio. r_1 is fixed at 1 while r_2 varies from 0 to 0.95.

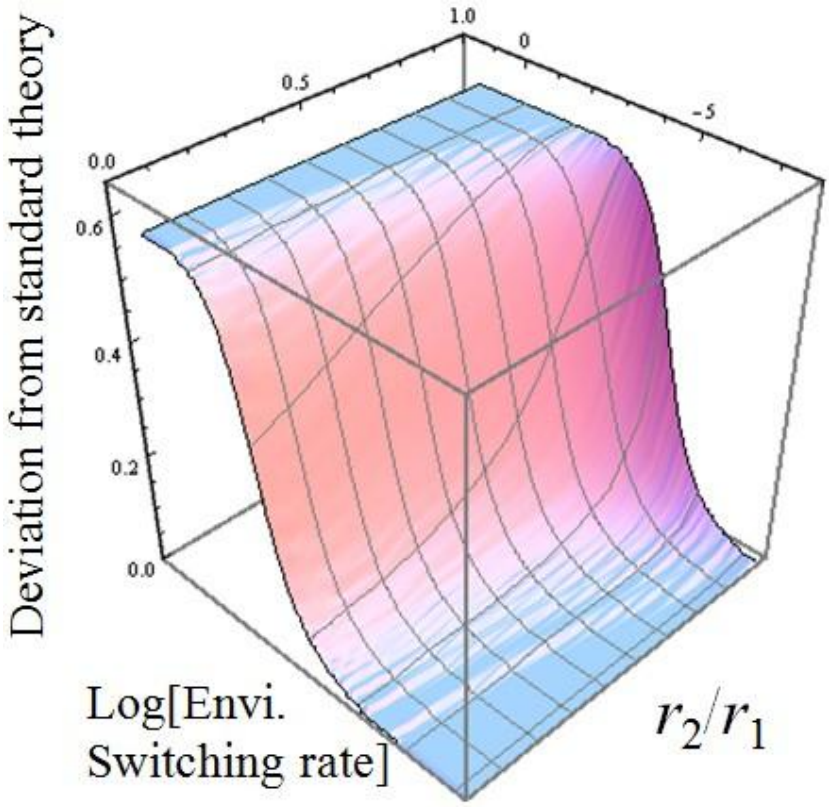

Figure 11 | Deviation of optimal phenotypic switching rates from predictions of the standard theory as a function of the environmental shifting rate and the growth rate ratio. It is defined as (optimal phenotypic switching rate - environmental shifting rate)/ environmental shifting rate.

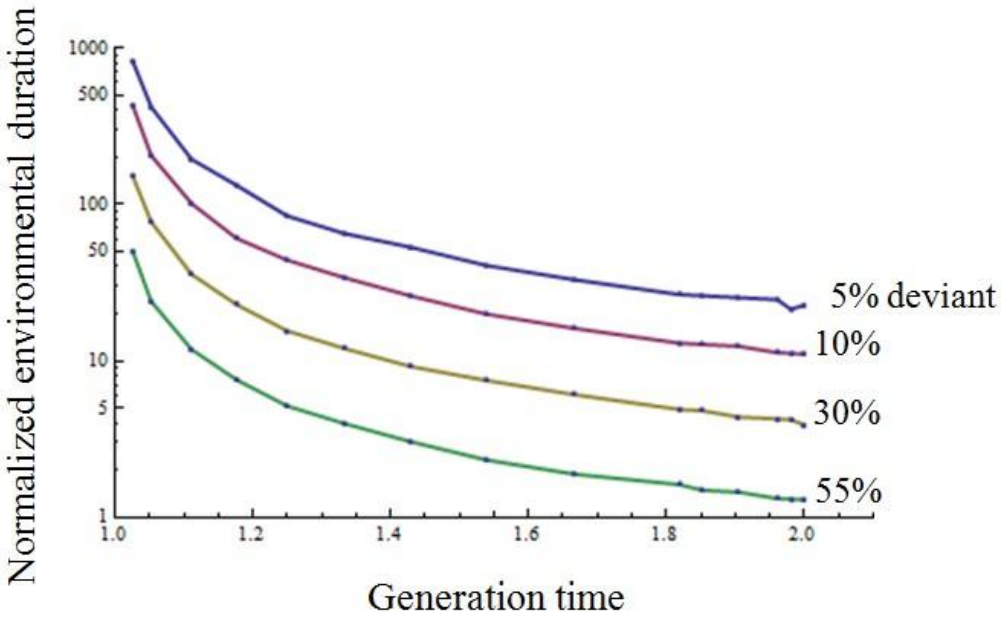

Figure 12 | Contours of deviant optimal phenotypic switching rates as a function of generation time and environmental duration normalized to generation time. Generation time is calculated as $2/(r_1 + r_2)$, and normalized environmental duration is calculated as the reciprocal of environmental switching rate divided by the corresponding generation time.

A more tangible way of analyzing this deviation is to plot contours of deviation as a function of generation time and environmental duration normalized to generation time (**Fig. 12**). It is obvious that when the environmental duration is about or less than ten (four) times the organismal generation time, the optimal phenotypic switching rate is at least 10% (30%) faster than the standard prediction. In the calculation, r_1 is fixed as 1, and r_2 varies from 0 to 0.95. As r_2 becomes closer to r_1, the generation time, $2/(r_1 + r_2)$, decreases, and the regime of deviation extends to longer environmental durations. In conclusion, while large deviation only appears when the growth rate variability across different environmental states are small and the environmental durations are relatively

short (the green curve in **Fig. 12**), mild and significant deviation is present globally at any condition (the blue and purple curve in **Fig. 12**).

Compare responsive sensing and bet-hedging. Another strategy in dealing with changing environments is responsive sensing. Under the conditions that there is no delay and the cue organism senses perfectly predicts the environmental change, responsive sensing should out-compete bet-hedging because it does not incur any cost. In the following, the conditions mentioned above will be relaxed to compare responsive sensing and bet-hedging. For responsive sensor with delay of response or imperfect signal reliability, the growth rates of responsive sensor can be respectively written as

$$w = \frac{1}{2T}\int_0^{T/2}(r_2 + \delta + \frac{(r_1 - r_2)t^2}{1/\gamma + t^2})dt \tag{18}$$

and

$$w = r_1\eta + r_2(1-\eta) \tag{19}$$

where δ is a compensation for the asymptotic distance from the maximum growth rate ($\delta = (r_1 - r_2)[1 - T^2/(1/\gamma + T^2)]/2$) at the end of an environmental duration, γ is the signal responding rate (assuming perfect signal reliability) and η is the signal reliability. With these formula, direct comparison between bet-hedger and responsive sensor becomes possible. As shown by **Fig. 13**, delay of response to signal does increases bet-hedger's advantage but only at low signal responding rates. Interestingly, increasing the growth rate differentials (r_1-r_2) increases the relative advantage of bet-hedger (The

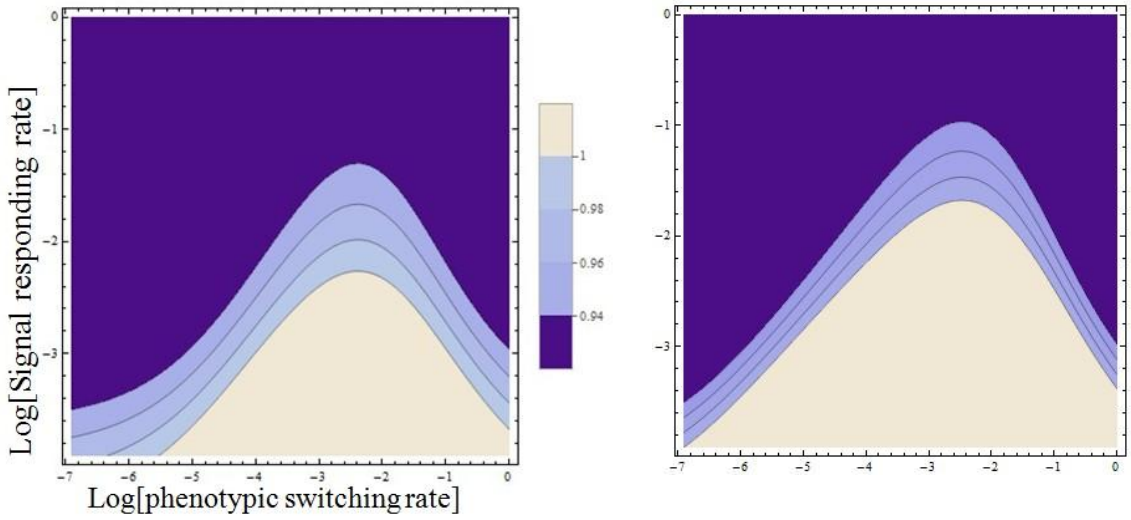

Figure 13 | Competition between bet-hedger and responsive sensor with response delay. r_1 is fixed as 1 for both panels and r_2 is 0.4 and 0.1 for the left and right panels respectively. Contours denote growth rate ratios of bet-hedger over responsive sensor. The environmental duration is fixed at 14. Legend is the same for both panels.

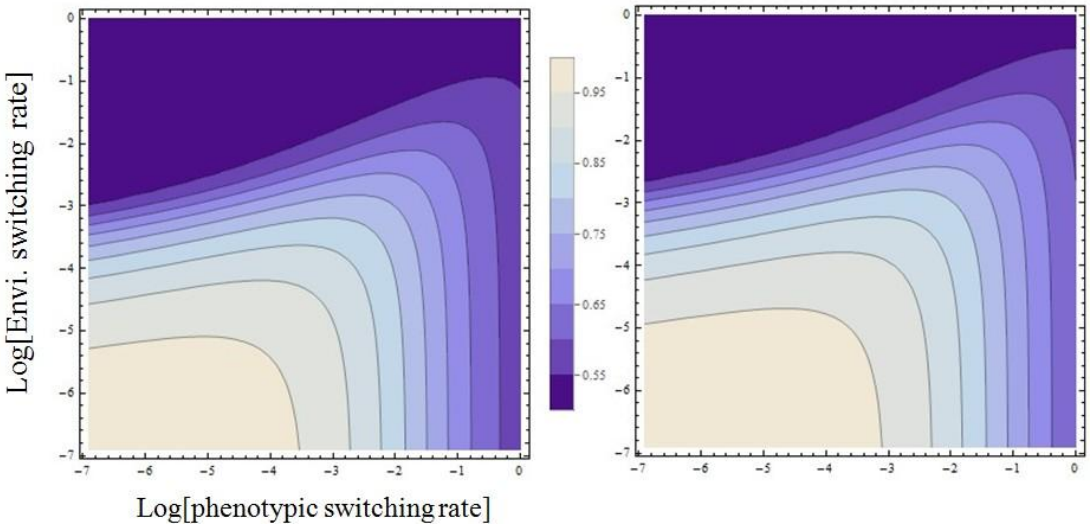

Figure 14 | Competition between bet-hedger and responsive sensor with imperfect signal. r_1 is fixed as 1 for both panels and r_2 is 0.4 and 0.1 for the left and right panels respectively. Contours denote the signal reliability levels at which bet-hedger and responsive sensors are equal in fitness. Legend is the same for both panels.

light region increases from the left to right panels, **Fig. 13**) . The same trend is observed for the case of imperfect signal (**Fig. 14**). Consistent with larger fitness advantage of bet-hedger over passive observer at infrequently shifting environment, precise information about the environment is needed for the responsive sensor to out-compete bet-hedger at low environmental shifting rates.

In conclusion, the dynamic theory of bet-hedging identifies an intermediate range of environmental shifting rates on the order of one hundredth to one tenth of growth rate. While this range bears large relevance to biological reality, it also carries systematic deviation from the prediction of the standard theory (**Fig. 12**), i.e., the optimal phenotypic switching rate shall be fine-tuned to the environmental switching rate. Indeed, simulation shows that the relative advantage of bet-hedging, passive observer and responsive sensor is contingent upon a set of parameters such as growth rate differential between different states, environmental switching rates, signal responding rate and signal reliability. In general, large growth differentials and infrequently shifting environments favor bet-hedging. In environments with intermediate range of shifting rates, parameters of competition, e.g., signs and/or magnitude, change dynamically and dramatically, rendering predictions on adaptive values of different strategies difficult.

3.3 Experimental tests

Intense efforts have been devoted to build an experimental system to test some crucial predictions made by the dynamic theory of bet-hedging. The challenge is to build a bet-hedging strain whose phenotypic states lead to environment-dependent differential growth.

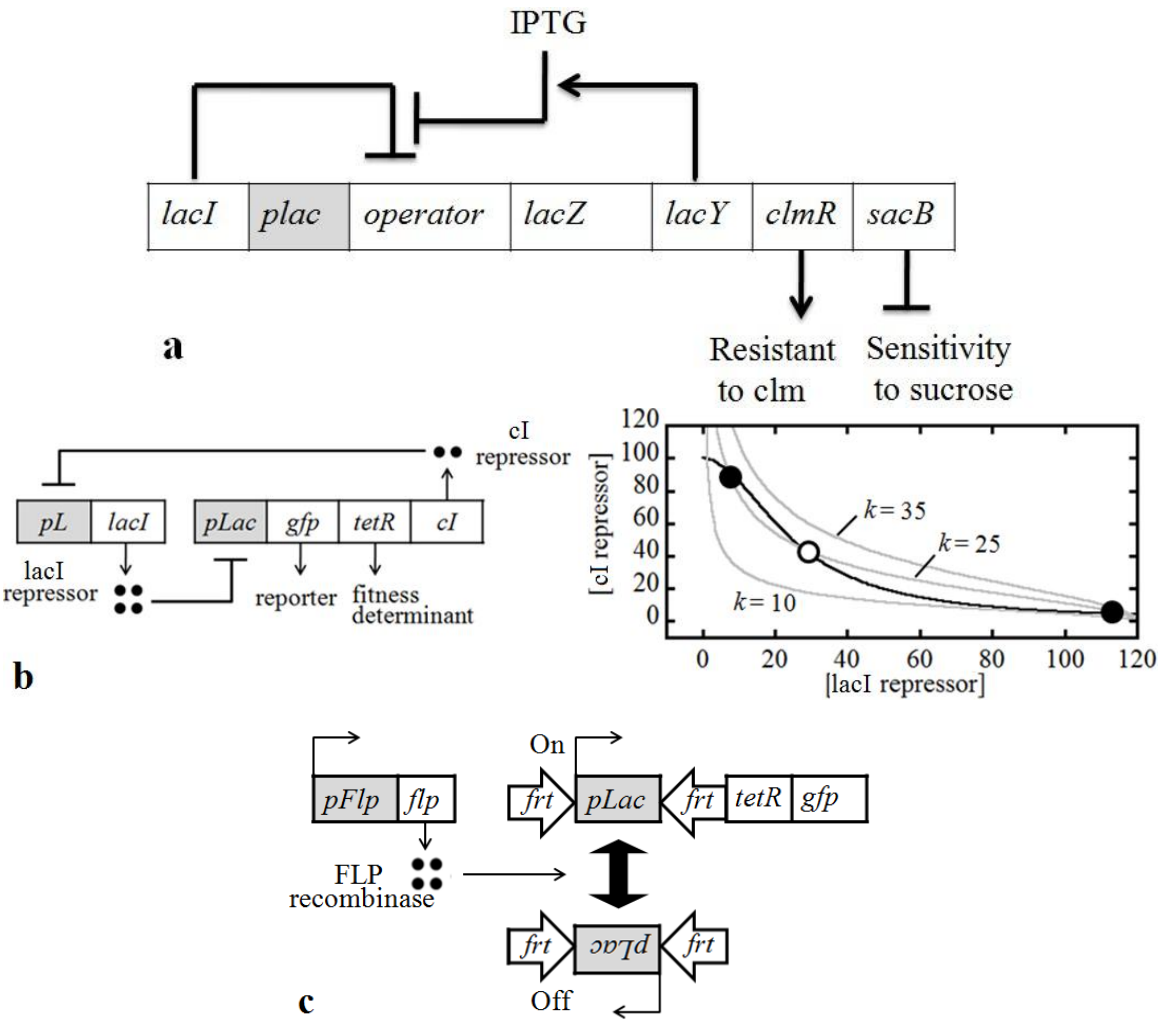

Figure 15 | Evolution of construct designs. **a.** Bistable expression of *lac* operon due to *lacY*-IPTG-*lacI* positive feedback. clmR and sacB confers resistance and sensitivity to chloramphenicol and sucrose respectively. **b.** Bistable toggle switch(Gardner et al., 2000). Expression of *tetR* is beneficial at the presence of tetracycline and detrimental at the presence of bleomycin. Gray boxes indicate promoters. The emergence of bistability. In the phase plane, the black and gray isoclines indicate the equilibrium concentrations of cI repressor and lacI repressor respectively. As the affinity of cI repressor to *pL* promoter, *k*, changes, the two isoclines can have either one (*k*=10 and *k*=35) or three (*k*=25) intersections, corresponding to monostable and bistable states of the system. The filled and empty circles indicate the stable and unstable equilibriums for *k*=25. Similar analysis can be done to the genetic circuit in **a**. **c.** Phase variation-based bistable expression circuit. *tetR* is fused to *gfp* so that the reporter faithfully reports the expression state of the fitness-determining gene. Catalyzed by FLP recombinase, the promoter constantly flips between on and off states reversibly(Friedland et al., 2009).

3.3.1 History of strain construction

In the past four years, the construct design itself experienced drastic evolution. The first one is based on the natural bistability of *lac* operon (**Fig. 15a**). Expression of *lacY* produces permease that brings IPTG into cells which in turn improves expression of the *lac* operon, completing a positive feedback loop. Literature reports that at certain critical extracellular concentration of IPTG, an isogenic population would partition to two phenotypic groups, expressing or not expression *lac* operon(Santillán et al., 2007). However, this design did not work because the range of IPTG concentration is too narrow and no stable switching between the phenotypic states was observed.

A second design (**Fig. 15b**) was based on the first published synthetic genetic circuit: a genetic toggle switch(Gardner et al., 2000). Again, IPTG needs to be tuned precisely for the bistability to appear. Indeed, I never observed any bistability from this construct, presumably due to the difference between being plasmid-borne (the published construct) and chromosome-borne (my construct). The third design (**Fig. 15c**) utilizes phase variation mechanism, whereby a site-specific recombinase reversibly changes the orientation of a segment of intervening DNA between two recognition target sites. This strain stably maintains bimodal distribution of reporter *gfp* gene.

3.3.2 Material and methods

Strain construction. The genetic circuit construction consists of two synthetic operons: the effector operon (**Fig. 15 c**, promoter and *tetR-gfp* fusion gene, including the two *frt* sites); the recombinase operon (promoter and FLP recombinase gene and its temperature-

sensitive repressor *cIts*). The same construction approach applies to both: synthesize the operon by stitching together different pieces (e.g., genes, promoters, *frt* sites) using fusion PCR technique (Szewczyk et al., 2007). A pair of primers (5' and 3' ends) for each piece were designed such that the 3' primer for one piece had ~30 base piece overlap with the 5' primer for its immediate downstream piece. Individual pieces are PCR amplified from independent sources (plasmids for *tetR*, *gfp*, *FLP*/*cI*, *frt*; genomic DNA for the rest). In addition to the components shown in **Fig. 15 c**, 1 KB up- and downstream the operon from targeted genomic context were also PCR amplified for homologous recombination in later steps. For the recombinase operon, a kanamycin cassette was also amplified and will be incorporated to the circuit to serve as the selective marker in the later step of chromosomal integration.

All products were quantified by comparing band intensity to a known marker (1 KB ladder, NEB) after running electrophoresis. They—the complete set of components for either of the operons—were mixed together with equal molar ratio in a PCR mix as templates and each about 20 ng in a 50 µl reaction. DNA polymerase Phire Hot Star II (ThermoFisher Scientific) was used and the reaction was set up following manufacturer 's instruction. PCR program followed the published fusion PCR program (Szewczyk et al., 2007). The overlap between primers allows extension of DNA polymerization of one piece into its neighbor during PCR reaction, at the end resulting in an intact composite chuck of DNA consisting the desired operon and up- and downstream sequences homologous to the genomic locus intended for integration (*lac* operon in this case). Product from fusion PCR reaction was gel purified with GeneJET Gel Extraction Kit

(ThermoFisher Scientific) to get rid of non-specific DNA species.

Lambda-Red method (Datsenko and Wanner, 2000) was used to integrate the engineered operons into the chromosome. Briefly, *E. coli* K-12 strain MG1655 was made chemically competent following standard procedure (Sambrook, 2001) and transformed with plasmid pKD46 (Datsenko and Wanner, 2000). Colonies were selected from LB agar plate (10g tryptone, 5g yeast extract, 10g NaCl, 15g agarose per liter, Fisher Scientific) with 50 µg/ml ampicillin after overnight incubation at 30°C to inoculate a fresh liquid LB medium. After growth overnight at 30°C, the culture was diluted 100 times into a fresh LB culture with 20 millimolar arabinose (Sigma-Aldrich) for induction of enzymes for homologous recombination. Cells were harvested by centrifugation and washed three times with ice-cold 15%(w/v) glycerol solution. Finally, 20 ng of insert DNA were mixed with 50 µl of competent cells for electroporation (1.8 kV, 5 ms, 10 mm cuvette, MicroPulser^{TM} Bio-Rad) . After two hours shaken at 37°C in SOC medium (2%(w/v) tryptone, 0.5%(w/v) yeast extract, 10mM NaCl, 10mM $MgCl_2$, 20mM Glucose, Fisher BioReagents), cells were plated on LB agar plates with appropriate antibiotics (7.5 µg/ml tetracycline for effector operon construct; 10 µg/ml kanamycin for recombinase operon construct). This procedure was applied to the operon constructs one after the other using to the same host strain. Fixed on and off strains were prepared similarly.

Competition and flow cytometry analysis were essentially the same as in chapter 2, except replacing minimal Davis media with Hi-Def Azure Media (rich defined, TECKNOVA) and chloramphenicol with bleomycin.

3.3.3 Bistable expression

The phase variation-based construct is so far the simplest and most reliable design of bistable gene expression system. Instead of depending on complex non-linear dynamics of feedback architectures such as found in the first two constructs (**Fig. 15b**, right panel), the bistability of this construct is the direct consequence of recombination reaction. In its essence, switching between on and off states is a process of mutation. It is deterministic in the sense that there are only two fixed genotypes (on and off) but stochastic because realizations of the switching folllow something close to Poisson distribution.

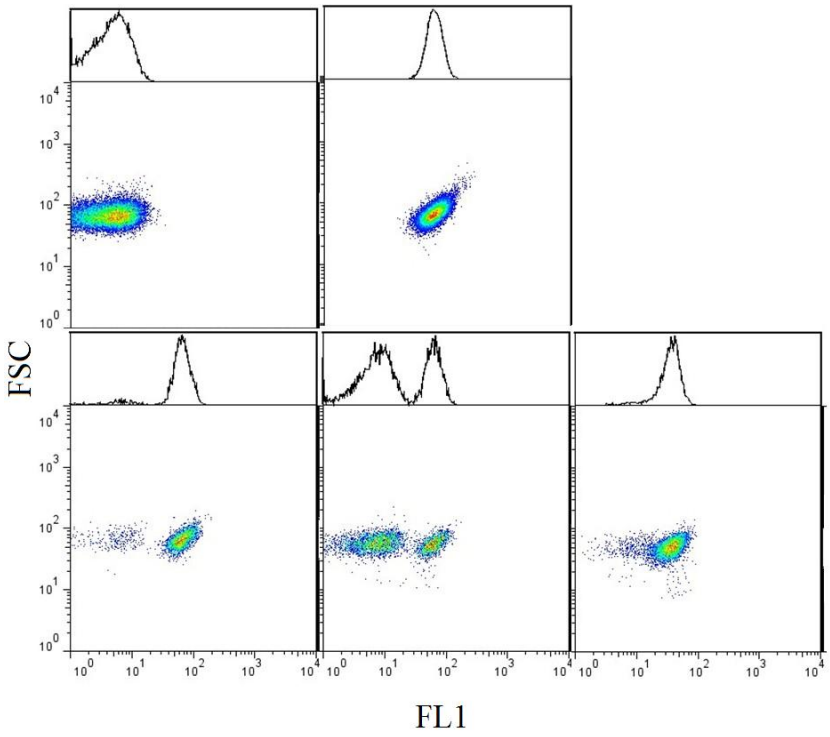

Figure 16 | Representative behaviors of the bistable system. Flow cytometry data display forward light scatter (y-axis, cell size signal) and fluorescent channel 1(x-axis, GFP signal). The top two are non-bistable strains fixed at off (left) or on (right), whereas the bottom three are infrequent switcher(still in the process of equilibration), medium speed switcher and fast switcher (from left to right). Note that the fast switcher does not show two peaks because the time scale of promoter flipping overlaps with the time scale of gene expression/dilution/degradation.

By mutating the recombinase, it is possible to control the switching rates (**Fig. 16**). Fortunately, the recombinase chosen (FLP) has been a model system in the studies of DNA recombination, so there exists a library of well-characterized mutants thanks to decades of research(Lebreton et al., 1988). My experiment confirmed that each mutant stably maintains its own characteristic switching frequency and no loss of switching has been observed for as long as 50 generations.

3.3.4 Competition

With the bistable and phenotype-fixed strains, now competition can be done between them to test theory predictions. The same T5 phage-based experimental techniques as used in chapter 2 can be used here to count the numbers of competitors using flow cytometer, except replacing YoPro-3 with ToPro-3 as the stain for the T5 phage sensitive competitor. Emitting far-red signal (FL4 channel) and having no overlap with GFP signal, ToPro-3 allows simultaneous and orthogonal measurements of phenotypic states and competitor abundances (**Fig. 17**, bottom).

As shown in **Fig. 17** top, the bistable strain out-competes both on and off strains, demonstrating directly the absolute advantage of bet-hedger over passive observers. Close look at the curve for competition with the on strain reveals that it gradually loses its advantage over the bistable strain in the environment with tetracycline. This contradicts the model prediction, indicating there is some unknown factor that interferes with competition. Preliminary diagnosis suggests physiology of the on strain changes gradually on the time scale of one complete competition experiment (~50 generations)

due to continuous overexpression of *tetR*.

In conclusion, a model of bet-hedging was developed that identified a biologically relevant region where standard theory fails. The reason for this is that the standard theory assumes the equilibrating phase at the arrival of a new environment is short enough to safely ignore so that matrix analysis can be applied and elegant analytical results can be obtained. Based on my explicit simulation that includes dynamics of the equilibrating phase, this assumption excludes a range of significant scenarios.

With competition experiments using the engineered bacterial strain, I demonstrate directly that stochastic gene expression can be a bet-hedging mechanism and that bet-hedging asserts extraordinary evolutionary advantage in changing environments.

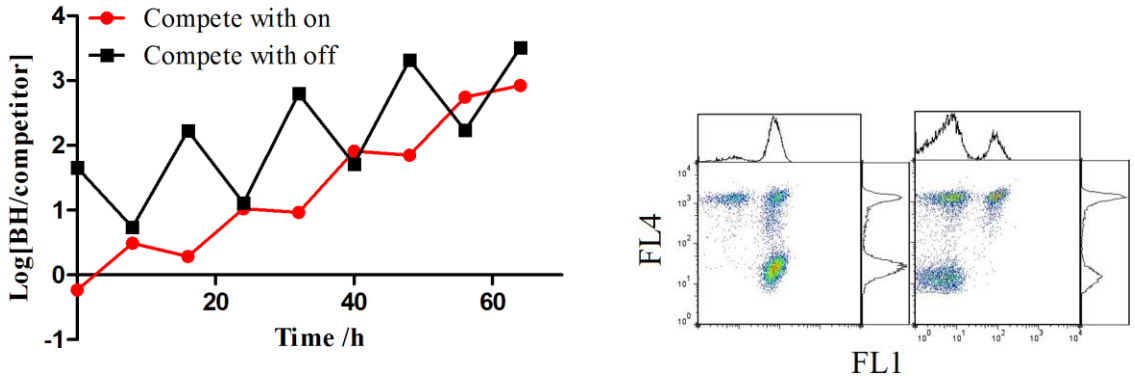

Figure 17 | Competition between bet-hedger and passive observer (on or off). Left, mixed populations of the bistable strain and either on (red) or off (black) strains experience environments alternating between the presence of tetracycline (even segments) and bleomycin (odd segments) every eight hours. Concentrations of antibiotics are the same for both competition experiments. Right, flow cytometer measures precisely the phenotypic state and cell identity with single cell resolution. FL4, fluorescent channel 4, measures ToPro-3 signal.

Chapter 4

Experimental evolution in fluctuating environments

Life is product of constant compromise among competing needs. A fundamental concept in life science, trade-off has been invoked in biological complexities at all levels (Allouche et al., 2012; Behrends et al., 2014; Keller et al., 2014; Lan et al., 2012) As the ability to cope with environments increases during evolution, functions carried out by life diversify. An inevitable consequence is that the performance in one function is limited by those of some others, given material (Kleiber, 1947; Mole and Zera, 1993) or structural (Chandra et al., 2011; Lan et al., 2012) conservation. Thus, simultaneous optimization in all functions is inhibited. Fitness is the ability of organisms to propagate, and results from the synergy of multiple functions (ARNOLD, 1983). As organisms adapt to their environments, the functions are compromising with each other along the direction toward fitness increase.

Theory (Nagrath et al., 2007; Shoval et al., 2012) anticipates performance of functions to be confined to a small subset of the phenotypic space, namely Pareto front. On such front, the hard bound of trade-off is met and fitness approaches an effective optimum presumably due to long term effect of natural selection. As this model stresses the consequence of restrictive force of trade-off in hindsight, it remains elusive how constraints interact with proximate and ultimate mechanisms (Mayr, 1961; Tinbergen, 1963) of life and thus become generative. Empirically, although data abound in support of negative correlation between functions (Berenbaum et al., 2007; Messina and Fox, 2001; Rose and Charlesworth, 1981), it only implies trade-off and is subject to alternative

conceptual (Agrawal et al., 2010) or methodological (Edelaar, 2013) interpretations. This is because causal establishment of trade-off is challenging.

Logically, trade-off can also drive organisms to explore alternative solutions for the benefit of fitness increase. At the same time it sets boundary for organisms' capability, trade-off could force them to constantly explore ways of breaking, provided there is a strong fitness increase of doing that. In this process, new biological complexity might emerge in the form of novel solution to overcome the limit. Unfortunately, this possibility remains entirely unexplored by scientific community.

This chapter presents an example where evidence for trade-off was first captured and a novel physiological program emerges in the face of trade-off, which alters organismic lifestyle. A model thus inspired precisely demonstrates how the presence of trade-off can facilitate its own breaking likely via novel biological mechanisms.

4.1 Materials and methods

Strains and media. The ancestral strain is *Escherichia coli*-K12 MG1655 from the Coli Genetic Stock Center at Yale. Note that under the strain name MG1655, there are a several entries, only one of them (CGSG# 8237) is motile and was chosen in this research. The others might have IS5 element deleted in the promoter region of the FlhDC operon that encodes two master regulators of chemotaxis and flagellum biosynthesis. The presence of this insert has been shown to induce motility (Barker et al., 2004). Bacteria were grown and evolved in Tryptone Broth (TB) (10g $NaCl_2$, 5g tryptone per liter; Fisher BioReagents) unless specified otherwise. Strains were isolated by streaking

for single colonies in Luria-Bertani (LB, 10g $NaCl_2$, 5g yeast extract 5g, 10g tryptone per liter; Fisher BioReagents) agar plates (12g agar per liter; Fisher BioReagents).

Experimental evolution. *E. coli* cells were selected for growth rate and chemotaxis in a fast-paced cyclic environment. From a single colony, the ancestral strain was grown overnight at 30°C to full density and diluted 1000 times to each of five 18 mm sterile glass tube (Pyrex) containing one ml TB. The five cultures were treated as replica of each other. They were incubated at 30°C and shaken at 250 rounds per minute. 10 .5 hours after the inoculation, 50 µl of each culture was diluted into 250 µl of washing buffer (2g KH_2PO_4,10g K_2HPO_4 and 29.2 mg ethylenediaminetetraacetic acid (EDTA) per liter, Sigma-Aldrich). It was centrifuged with 3000×gravity for 3 min, the supernatant was discarded, and the pellet was re-suspended in 300 µl of washing buffer by pipetting up and down gently to minimize flagellar damage. 150 µl of the suspension was transferred to a well in a sterile 96-well microplate (BD Falcon). Having loaded all five samples, the plate was erected on one side so that it became perpendicular to the bench surface and the small amounts of liquid would retain inside the wells due to surface tension. Glass micro-capillary (0.8 mm inner diameter × 75 mm, Drummond) was heat-melted at one end to seal the opening. After cooled at room temperature, the capillary was flamed over Bunsen burner briefly and the open end was immediately submerged into TB. Having cooled at room temperature, the capillary would have absorbed ~5 µl of liquid inside. Washing buffer was pipetted to rinse off carryover medium on the outer surface of the capillary. The open end was submerged into the pond in the well and the whole system was

incubated at 30°C for chemotactic competition to occur. After 30 min, the capillary was pulled out of the well and rinsed with washing buffer to get rid of cells carried on the outer surface. The liquid inside together with cells attracted into it were pushed into a fresh TB medium contained in a glass tube by flaming the capillary briefly. This inoculated culture was then incubated at 30°C and shaken at 250 rounds per minute, closing the loop of experimental evolution. The growth-capillary selection loop was repeated 126 times (9 weeks) continuously. At the end of every week, 1 ml of culture was taken from each tube and diluted with 80% sterile glycerol to the final glycerol concentration of 16%. The diluted cultures were stored at -80°C as archives. For each archived culture, 6 single strains were randomly picked from single colonies streaked on agar plate. Each strain was characterized in growth rate and chemotactic ability.

Measurements of growth rate and chemotactic ability. Ancestral strain was treated as previously described to isolate T5 phage-resistant mutant ($T5^r$). This mutation has been shown to be neutral(Lunzer et al., 2002). Each of the isolated and $T5^r$ ancestral strains was grown overnight in TB liquid medium before being 1000×diluted into a fresh medium. Samples were taken from the culture at the 4^{th} and 5^{th} hour after dilution and assayed using flow cytomter (BD FACSCalibur) in order to measure cell density. Growth rate (r) is calculated using the following formula: r = (Log[cell density at 5th hour] - Log[cell density at 4th hour])/1hour. This formula assumes the populations were at exponential phase during the time period considered. This was confirmed by experiment.

At the 11^{th} hour, sample was taken from the culture, diluted, centrifuged, and re-

suspended the same way as in experimental evolution. Suspension from each of the isolated strains was mixed 1:1 in volume to the suspension of the $T5^r$ ancestral strain. The mixture was treated the same as in experimental evolution for capillary selection. After 30 min of incubation, the capillary was rinsed with washing buffer to get rid of cells on the outer surface and the liquid inside was pushed into 200 µl of washing buffer by flaming the capillary briefly. This sample (post-incubation) as well as the saved pre-incubation mixture were treated as following to measure the ratio of the isolated over $T5^r$ ancestral strains. For the pre-incubation mixture, 20 µl was diluted into 180 µl washing buffer. To this diluted sample was added 2 µl of 12.5 mg/ml chloramphenicol (Sigma-Aldrich), 20 µl of LB, 20 µl of T5-phage lysate (titer ~ 10^9 phage particles/µl), 1 µl of TO-PRO-3 stain (1mM solution in DMSO, Life Technologies) and 57 µl of 62.5 mM EDTA water solution. The post-incubation mixture was treated the same way except without the initial dilution. After vortex, these mixtures were incubated at 37°C for 30 min before being assayed by flow cytometer. For the isolated strains, which were naturally T5 phage-sensitive, cells were attacked by phage and cell membrane was depolarized so that TO-PRO-3 stain would diffuse into the cell and bind double-stranded DNA. Upon excitation by the red laser of FACSCalibur (642 nm wavelength), the DNA-bound stain emits far-red fluorescent signal. Whereas, the $T5^r$ ancestral strain did not allow attack by T5-phage and thus gave no fluorescent signal. Under FL4 fluorescent channel of the flow cytometer, the mixed population would give a bimodal distribution with the fluorescent positive and negative sub-populations corresponding to the isolated and the ancestral strains respectively. Chemotactic ability is defined as c = (Log[ratio of

isolated over ancestral strains]|$_{\text{post competition}}$ - Log[ratio of isolated over ancestral strains]|$_{\text{before competition}}$)/0.5 hours. For each isolated strain, the experiment was done in three replica, and the growth and chemotactic ability were taken as their averages.

Construction of adaptive landscape. Competitions in the two stages of growth and chemotaxis contribute to fitness in a coupled way. The wild type *E. coli* was used as a common competitor for all mutants to measure their relative fitness. In a typical competition, assume wild type and the mutant were initially mixed 1:1 ratio, each with normalized population size $n_0 = N_0 / K$, where *K* is the carrying capacity of environment for bacteria. Competition for limited resource is commonly modeled as Lotka-Volterra equations(Gotelli, 1998):

$$\begin{cases} \dfrac{dm}{dt} = rm(1-m-w) \\ \dfrac{dw}{dt} = r_w w(1-m-w) \end{cases}$$

where *m* and *w* are normalized population sizes for the mutant and wild type at time *t*; *r* and r_w are their respective growth rates. Here two assumptions are made: 1) Both competitors have the same carrying capacity in TB; 2) There are no direct interactions between them and they compete only through depletion of common resource. The assumptions are legitimate to make, because all mutants and wild type are closely related to each other (a few mutations way from each other) and the selective regime used is insensitive to both carrying capacity and interactions between competitors. By algebraic transformation, the equations above are equivalent to:

$$\begin{cases} \dfrac{dw}{dt} = rw(1-w-wp) \\ \dfrac{dp}{dt} = (r-r_w)\,p(1-w-wp) \end{cases}$$

where $p = m/w$. Analytical solution for these equations is unknown. But, with r_w = 1.059478 as measured, the initial conditions (p_0 = 1, w_0 = 1/2500) and running time = 11 hours, we can numerically simulate $f = p_{11}$ as a function of r. We used the "NDSolve" function and default parameterization in Mathematica® 9.0.1.0 (Wolfram Research, Inc.) for the simulation. f gives the ratio of the mutant over wild type after 11 hours of growth competition; as the culture would then be subject to capillary selection in experiments, this number is used as the initial ratio for chemotactic competition. This leads to the equation $w = [Log(f(r)) + c/2]/t$ as discussed in the main text. This equation now precisely models the adaptive landscape for the experimental evolution.

Calculation of selective gradients in the adaptive landscape

With this adaptive landscape, we can study selective gradients along the two functional dimensions. Using the "Table" function of Mathematica, a grid of values for c and r are generated, covering the space traveled by the evolving population: c from -1 to 8 with incremental size of 0.2; r from -0.2 to 0.3 with incremental size of 0.025. Plugging this grid into w described above, a fragment of the landscape is mapped with (c_{ij}, r_{ij}, w_{ij}), i and j being the indexes for the simulated values of c and r respectivelys. Simply eyeballing the surface made of the points reveals that it is very smooth and approximates a

plane(**Fig. 18c**). Thus it is sensible to use averaged gradients to describe the general feature of the landscape. The average gradients are calculated as following:

$$\frac{\partial w}{\partial c} = \frac{\sum_j \frac{\sum_i w_{i+1,j} - w_{i,j}}{0.2(-1+\sum i)}}{\sum j}$$

$$\frac{\partial w}{\partial r} = \frac{\sum_i \frac{\sum_j w_{i,j+1} - w_{i,j}}{0.025(-1+\sum j)}}{\sum i}$$

Genomic sequencing. After systematic characterization across nine weeks of evolution in the isolates' growth rate and chemotactic ability, representative strains were chosen for genomic sequencing. Each strain was revived from the frozen archive and grown in LB medium overnight. One ml of the culture (8×10^8 cells) was processed using GeneJET Genomic DNA Purification Kit (Thermo Scientific) following manufacturer's instruction, yielding ~1 µg genomic DNA in 300 µl nuclease-free water. DNA library preparation was done using Nexterra XT DNA Sample Preparation Kit (illumina) and each strain was barcoded uniquely with an adapter sequence. Samples from all strains were pooled together and sequenced with HiSeq 2000 pair-ended 50 cycles (service provided by the Biomedical Genomic Center of University of Minnesota). The coverage for each isolate was ~160 times. Genomes were assembled and mutations were identified against the wild type *E. coli* using the Breseq pipeline (Barrick et al., 2009) with default parameter values.

For isolated strains, the "breseq" command was used; for evolved populations, the" --polymorphism-prediction" function was used.

Mutant reconstruction. For the week 9 isolate (W9), among the four mutations identified, the *fliA* was chosen for genetics reconstruction. Four crossover strains were made: ancestral genetic background with ancestral version of *fliA*, ancestral genetic background with W9 version of *fliA*, W9 genetic background with ancestral version of *fliA*, and W9 genetic background with W9 version of *fliA*. They were constructed as following. Starting from the promoter region of *dcyD* operon (an immediate neighbor to *fliA* operon), both upstream and downstream 1Kb sequences were PCR amplified separately (ancestral and W9 strains have identical sequence in this 2Kb region). The kanamycin resistance cassette from pKD13(Datsenko and Wanner, 2000) was PCR amplified. A fusion PCR(Szewczyk et al., 2007) was carried out to fuse the three fragments so that the kanamycin resistance cassette was sandwiched by the two genomically derived sequences. For each of the ancestral and W9 strains, the kanamycin resistance cassette was integrated at the genomic region between the terminator of *fliA* operon and the promoter of *dcyD* operon, following the lambda red-mediated homologous recombination method (Datsenko and Wanner, 2000). Briefly, the strain was transformed with pKD46 which expresses proteins required for homologous recombination. After cells were made electro-competent, 50 µl was mixed with 40 ng fusion PCR product and electroporated using MicroPulser Electroporator (Biorad, 1.8kV, 5 ms, 10 mm cuvette gap). Having recovered from incubation in SOC medium (2%(w/v) tryptone, 0.5%(w/v) yeast extract,

10mM NaCl, 10mM $MgCl_2$, 20mM Glucose, Fisher BioReagents) at 37°C for 4 hours, cells were plated on LB agar plates supplemented with 20 µl /ml kanamycin (Sigma-Aldrich). Single colonies were selected and saved for downstream experiments. At this point, both ancestral and W9 strains were tagged with kanamycin resistance marker near *fliA*. Next, P1 phage transduction(Miller, 1992) was used to introduce ancestral and W9 versions of *fliA* to W9 and ancestral genetic backgrounds respectively. The reconstructed strains were verified by Sanger sequencing at the *fliA* locus cycles (service provided by the Biomedical Genomic Center of University of Minnesota).

Measurement of swimming speed. Along the course of batch growth described above, a small fraction of the culture was withdrawn every one or two hours. For early hours (before 5^{th} hour after initial dilution), the sample was centrifuged mildly (1000×gravity) for 3 min, avoiding flagellar damage, and certain amount of supernatant was discarded to reach proper cell concentration. In late hours, cells were diluted with washing buffer accordingly. A simple and effective techniques of slide preparation was adapted (Staropoli and Alon, 2000): a full circle with diameter of 10mm was drawn with China marker on a slide (thickness: 1.0mm, size: 25×75mm, VWR), 2µl of the sample was pipetted inside the circle before the cover slip (thickness: 0.13mm, size: 18×18mm,VWR) was amounted. Air bubbles were avoided to create a homogenous and well-confined environment between the cover slip and the slide. The slides were viewed with Olympus XI 70 microscope equipped with SPOT Flex™ camera (16M CCD, Diagnostic Instruments, Inc.), with phase contrast field, 10×magnification in eye lens and

40×magnification in objective lens. For each slide, five seconds of video was taken at each of five different fields with 16 frames per second. The whole process was completed within 10min after sample withdrawal, so that the physiological state was not significantly disturbed.

Video clips were analyzed by Image-Pro® Plus 6.0 (Media Cybernetics, Inc.). The built-in filter function "Sobel" was applied to outline individual cells at each frame. "Count/Size" was used to identify and tag each cell with default parameter values. "Track Objects" was used to track trajectory of each cell. The automatically recognized trajectories were filtered by human inspection to get rid of false tracking. For each passed trajectories, the program returned velocity at each frame. The average of 50 frames was taken as the final swimming speed. Data from multiple fields with the same sample was pooled to collect enough trajectories (300-500) to calculate mean and standard error.

4.2 Results

4.2.1 Experimental observation

Here, with evolving laboratory populations of bacteria, I report an example where functional trade-off shapes evolutionary trajectories and leads to the emergence of a novel physiological program. Because both growth rate and chemotaxis—the ability to move up a gradient of nutrient—are energetically expensive (Macnab, 1996) and contribute to bacterial fitness (Freter and O'Brien, 1981), there must be a trade-off. To address this hypothesis, populations of *E. coli* experienced repeated alternations between a growth stage and a stage of capillary selection (**Fig. 18a**). The time scale of

environmental alternation (8 generations) being well below that of selective sweep, this experimental regime imposes a strong selection for simultaneous improvement in growth rate and chemotactic ability. With this dual selection, if the evolving population travels along a negative diagonal in the performance space, that will be the signature of trade-off (Agrawal et al., 2010) (**Fig. 18 b**).

For conceptual and experimental convenience, functions are defined in relative terms. Relative growth rate (*r*) is the difference between the exponents of growth for the mutant and the ancestor. Relative chemotactic ability (*c*) is the logarithmic fold change in population size of the mutant compared to the ancestor, when moving up a nutrient gradient in one hour. Based on competition within a single selection cycle, fitness is defined by the equation: $w = [Log(f(r)) + c/2]/t$, where *t* is the overall duration of competition, and *f* is the ratio of the mutant to the ancestral populations at end of the batch growth and is a function of *r*. In my experiments, all variables can be arbitrarily and precisely tuned, except for *c* and *r*. With these two parameters freely mutable as intrinsic properties of bacteria, $w(r,c)$ determines explicitly the adaptive landscape of this system (**Fig. 18b**).

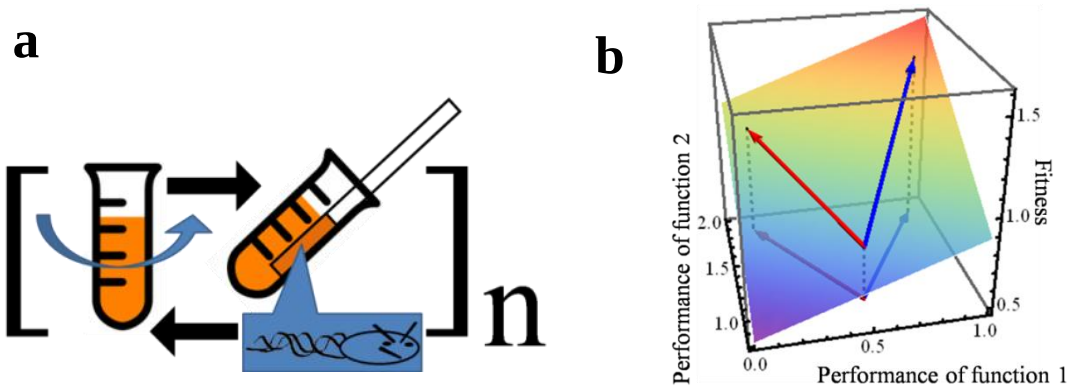

Figure 18 | Experimental evolution to test trade-off. **a.** Batch culture was shaken and incubated at 30 °C. Eleven hours later, when cells were still in late exponential phase, capillary carrying fresh medium was lowered into the culture to attract the chemotactically active cells. **b**. The concept for the test of trade-off is best demonstrated by a two-function adaptive landscape. The landscape topology is explicitly defined by the experimental setup.

Initiated with the wild type *E. coli* strain MG1655, the selection cycle was repeated 126 times, spanning 9 weeks, with ~1000 generations elapsed. As shown in **Fig. 19a**, the evolving population traveled across a substantial area in the performance space, leaving a complex trajectory. There were three major periods of phenotypic evolution: the early (the first two weeks), middle (week 2 to 7) and late (week 7 to 9) periods.

For the early period, chemotactic ability was substantially increased (analysis of variance, $P < 0.0001$) with insignificant growth rate improvement (analysis of variance, $P = 0.16$), suggesting wild type *E. coli* might have not evolved to the limit of trade-off or the functions were buffered in a high dimensional Pareto front (Shoval et al., 2012). Indeed, growth rate evolves quickly during evolution in the absence of capillary selection (data not shown) and the selective gradient along the growth rate axis in the current adaptive landscape is much steeper than chemotaxis (0.603 vs. 0.087). These indicate the

domination of adaptation by chemotactic response was due to larger phenotypic impact of chemotactic mutations rather than their richer supply.

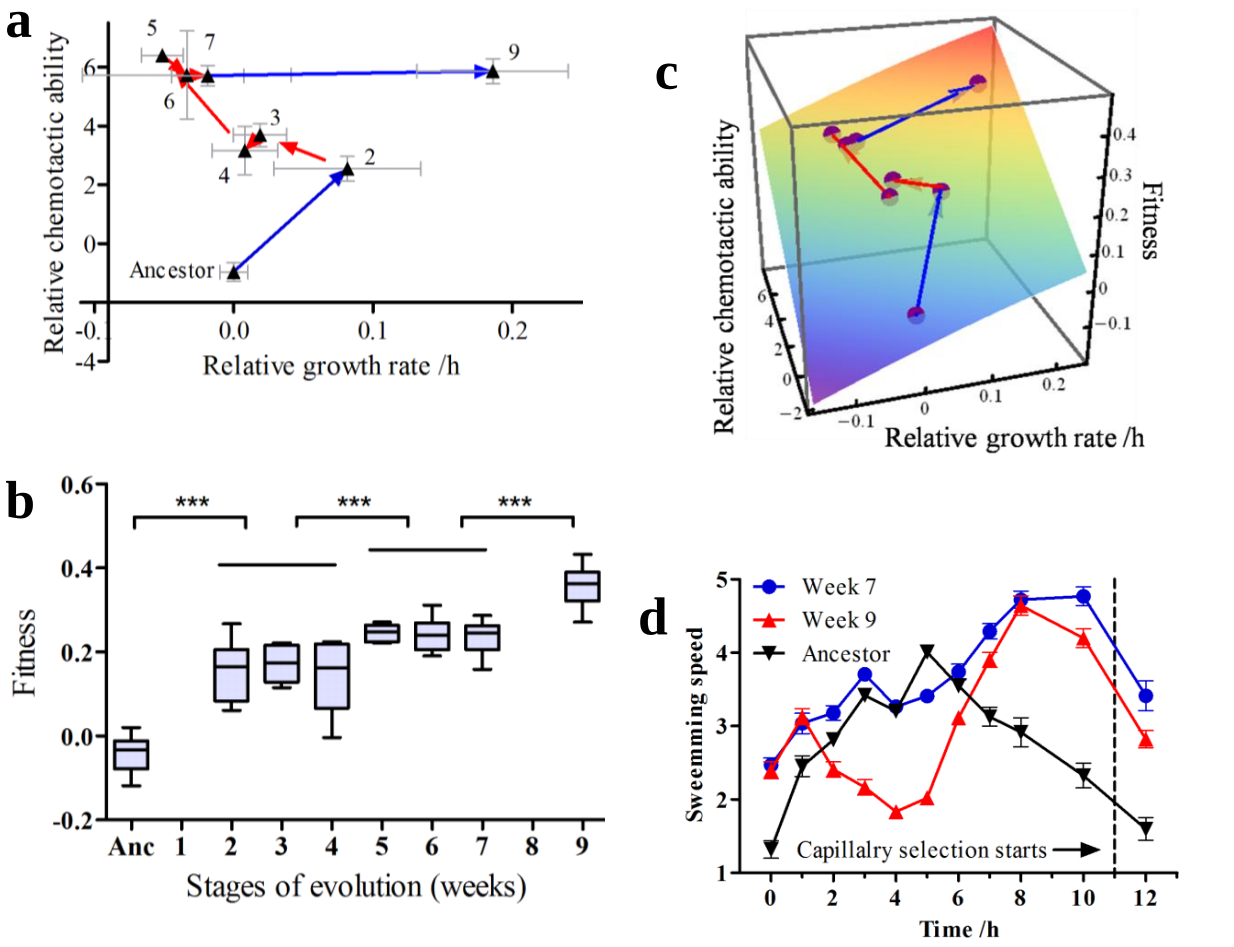

Figure 19 | Evolutionary trajectories on defined adaptive landscape. **a.** Phenotypic evolution of the evolving population in the performance space of growth rate-chemotactic ability. Number indicates stage of evolution in weeks. Each point represents an average of six isolates randomly picked from the corresponding week. Error bar, one standard error. **b.** fitness kinetics across 9 weeks of evolution. For each isolate, fitness is derived by plugging the measured r and c into $w(r,c)$ (Materials and methods). *** indicates $P < 0.0001$, analysis of variance. Whiskers, 5-95 percentile. **c.** The evolutionary trajectory is mapped onto the adaptive landscape computed according to the experimental setup. **d.** Motility kinetics in one batch culture of representative isolates from different stages. Color indicates week of isolation: black, blue and red for 0, 7, 9 weeks into evolution. Dashed line indicates the time point for capillary selection during experimental evolution.

Signature of trade-off came from the middle period. Comparing week 2 and the pool of week 5 and 6, growth rate dropped by 14.2% (P = 0.029) while chemotactic ability increased 2.69 folds (P = 0.0018). Not only did the population travel along a negative diagonal in the performance space, the fitness also increased (**Fig. 19b**). But the magnitude is only minimal and the pace slow, regardless of the large phenotypic change and strong selective force already demonstrated in the early period. Another evidence consistent with the trade-off is that isolates with low growth rate and high chemotactic ability showed hyper-motility across the whole batch growth (**Fig. 19d**).

An apparent breakage of the trade-off appeared in the late period, with dramatically improved growth rate (by 23.5%, P = 0.004, comparing week 5 and 9) while maintaining high chemotactic ability. Fitness also earned a release from 5 weeks near stagnancy in the middle period. A look at the swimming speed kinetics spares the counter-intuitive breakage of trade-off (**Fig. 19d**). In contrast to the ancestor who gives a shape of triangle characteristic of wild type (Amsler et al., 1993), with swimming speed peaking around the 5^{th} hour after dilution, representative isolates from week 7 and week 9 evolved distinct strategies to deal with the dual selection. While de-inhibition of flagellar activity by the isolate from week 7 produced global increase of swimming speed, from early log to stationary phases, the isolate from week 9 exhibited a more subtle reprogramming of the kinetics with substantial deferral of peaking. Specifically, swimming speed is kept low during the phase of batch growth, saving energy for high growth rate; but it catches up when the point of capillary selection is approaching. This new program decouples growth rate from chemotactic ability, thereby bypassing the

trade-off and enabling the evolving population to explore area of the adaptive landscape previously unachievable.

4.2.2 Genetic mechanisms of the phenotypic adaptation

To gain mechanistic insight, we sequenced the genomes of a representative strain from week 7 (**Tab. 4**) as well as populations at week 4 and 9 (**Tab. 5**). By comparing the isolate against the populations, we identified two adaptive mutations (type I): one is a non-synonymous mutation in *yahA* and another in the promoter region of *yegE*. Both genes encode enzymes that regulate concentration of intracellular cyclic di-GMP. In fact, previous work has established that this secondary messenger negatively regulates flagellar activity in *E. coli* (Boehm et al., 2010; Pesavento et al., 2008). Comparing the mutant with the ancestor in kinetics of swimming speed across full length of batch growth (**Fig. 19d**), it is obvious that these mutations relieved the suppression of motility. Experiments confirmed that swimming speed determines chemotactic ability (**Fig. 20**). Now a coherent picture of the trade-off emerges: as strong selection picks up mutations that de-inhibit flagellar activity in the cyclic di-GMP pathway, the librated motors consume substantial amount of energy. Beyond certain threshold, growth rate is retarded.

We sequenced the genome of the isolate from week 9 (**Tab. 4**). By comparing it against those of the populations (**Tab. 5**), we identified possible causal mutations for the observed phenotypes (type II): two non-synonymous mutations, one at *fliA* and the other *rpsC*. *FliA* encodes the chemotaxis-specific sigma factor, and the mutation (R220W) occurs at the DNA-binding domain (Sorenson et al., 2004), where the sigma factor

recognizes and interacts with promoter, initiating transcription. *RpsC* encodes 30S ribosomal subunit 3S. We decide to focus on the effect of *fliA* mutation with knock-in and -out genetics. As shown in **Fig. 21**, this mutation does cause the deferral of peaking of swimming speed in both genetic backgrounds of the ancestor and the type II mutant.

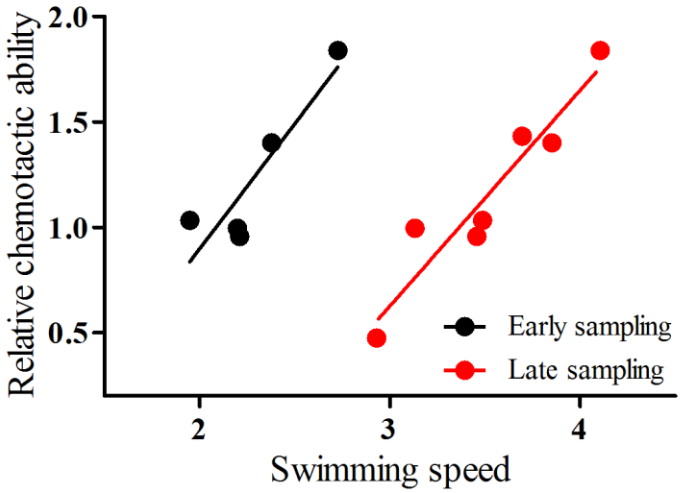

Figure 20 | Correlation between swimming speed and chemotactic ability. Each dot represents a different isolate. Cells were grown in a standard batch culture. Two hours (black) and eight hours (red) after inoculation, samples were taken for measurements. During incubation in capillary competition assay (30min), swimming speeds were determined within 20 min after sampling. For black points, $c = 1.187v - 1.478$, R^2 = 0.82; for red points, $c = 1.023v - 2.444$, R^2 = 0.90.

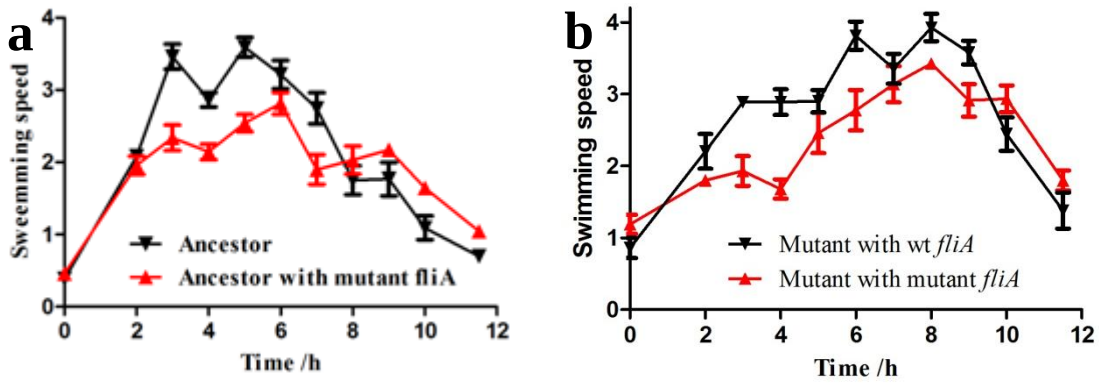

Figure 21 | Swimming speed kinetics of strains with the *fliA* mutation. **a**. Swimming speeds measured every one or two hours during a typical batch growth for the ancestor(black) and ancestor with *fliA* mutation. Overnight cultures were diluted 2500 times into fresh media at hour 0, then shaken at 30°C. At each time point, a small fraction was drawn to prepare slides, from which 5s-long video clips were taken with microscope. The unit is arbitrary unit of length per second. Each point represents the average of 300-500 individual cells. Error bars, one standard error. **b.** Empty circle indicates the type II mutant, four mutations away from the ancestor. Filled circle indicates indicates the type II mutant with the wild type version of *fliA*. For each strain, the speeds are normalized to its maximum value for the convenience of pattern comparison.). Each point represents the average of ~1000 individual cells. Error bar, one standard error.

While type I adaptation runs to the limit of cellular energy, type II gets around by temporally localizing growth and motility, becoming more fit while fundamentally transforming bacterial lifestyle. For wild type *E. coli*, the rapid decay of motility post mid-exponential phase conforms to a conservative life strategy: as food runs low, cells reduce motility and prepare to settle locally such as in the form of biofilm (Pesavento et al., 2008). The new motility program installed, cells now tend to be opportunistic—getting ready for exploration of new environments when the current one deteriorates.

In the genomes of individual isolates (**Tab. 4**), the mutations are not necessarily all adaptive because of hitchhiking . To get an idea of the population dynamics of the adaptation processes, we compared mutation frequencies in week4 and 9 for the coarse

dynamics of major polymorphisms. With strong selective pressure and short generations elapsed in our experiments, we expect to see large selective sweeps of a small number of mutations. If these mutations also appear in the isolate mutations, then it confirms that the isolate is representative of the adaption and we can focus downstream studies on these mutations. Then again, these narrowed set of mutations are not necessarily all adaptive because non-adaptive mutations might occurr in the genome before the adaptive ones. Symbolically, adaptive mutations $\subseteq$ sweeping mutations in the population $\subseteq$ mutations one single isolates. As shown **Tab. 5**, polymorphisms were dominated by two groups of mutations. For the group of mutations at *yegE, yahA*, upstream *CsiD*, the frequency dynamics of constituent mutations from week 4 to week 9 are synchronized, indicating they sat on the same genome. This is confirmed by their presence in a single isolate genome from week 7. The second group consists of mutations at *fliA, rpsC* and upstream *rbsK*. None of them were detected at week 4 but they swept to ~50% of the population at week 9.

We excluded the mutation between *rbsB* and *rbsK* from the candidate causal mutations for the phenotypes of interest, because the *rbs* operon is responsible for ribose catabolism, a terminal metabolic module (Lopilato et al., 1984). This leaves mutations at *fliA* and *rpsC* as type II mutations mentioned in the main text. For similar reasons, we exclude the mutation upstream *CsiD*, leaves mutations at *yegE* and *yahA* as type I mutations.

Table 4 | Complete mutations of representative isolates from week 7 and week 9

	Nucleotide change	Animo acid substitution or genomic context	Genes	Phenotypes
Week 7 isolate	G→T	G167C (GGT→TGT)	*yahA* →	c-di-GMP-specific phosphodiesterase
	G→T	L356L (CTC→CTA)	*dcp* ←	dipeptidyl carboxypeptidase II
	repeat_region (–) +4 bp	intergenic (-209/-52)	*udk* ← / → *yegE*	uridine/cytidine kinase/diguanylate cyclase
	repeat_region (+) +4 bp	intergenic (+113/-115)	*yqaD* → / → *CsiD*	orf, hypothetical protein/orf, hypothetical protein
	repeat_region (–) +9 bp	coding (1504-1512/2247 nt)	*ptsP* ←	PTS system, enzyme I, transcriptional regulator (with NPR and NTR proteins)
Week 9 isolate	Δ5,579 bp		*[gapC]–[ydcJ]*	*[gapC], cybB, ydcA, hokB, mokB, trg, ydcI, [ydcJ]*
	G→A	R220W (CGG→TGG)	*fliA* ←	flagellar biosynthesis; alternative sigma factor 28; regulation of flagellar operons
	C→T	E82K (GAA→AAA)	*rpsC* ←	30S ribosomal subunit protein S3
	repeat_region (+) +5 bp	intergenic (+86/-36)	*rbsB* → / → *rbsK*	D-ribose periplasmic binding protein/ribokinase

Table 5 | Polymorphisms measured at week 4 and week 9. Mutations with <5% frequency are not shown. Mutations are arranged from the most frequent down.

Week 4			Week 9		
Freq	Loci	Annotation	Freq	Loci	Annotation
90%	*udk* ← / → *yegE*	uridine/cytidine kinase/ diguanylate cyclase	59%	*yahA* →	c-di-GMP-specific phosphodiesterase
80%	*yqaD* → / → *CsiD*	orf, hypothetical protein/orf, hypothetical protein	58%	*udk* ← / → *yegE*	uridine/cytidine kinase/ diguanylate cyclase
74%	*yahA* →	c-di-GMP-specific phosphodiesterase	54%	*yqaD* → / → *CsiD*	orf, hypothetical protein/orf, hypothetical protein
37%	*yadL* ←	putative fimbrial protein	51%	*fliA* ←	flagellar biosynthesis; alternative sigma factor 28; regulation of flagellar operons
23%	*kdpD* ←	sensor for high-affinity potassium transport system	47%	*rbsB* → / → *rbsK*	D-ribose periplasmic binding protein/ribokinase
16%	*yobF* ← / ← *yebO*	orf, hypothetical protein/orf, hypothetical protein	44%	*rpsC* ←	30S ribosomal subunit protein S3
16%	*yobF* ←	orf, hypothetical protein	29%	*gltP* → / ← *yjcO*	glutamate-aspartate symport protein/orf, hypothetical protein
9%	*stfE* ←	side tail fiber protein homolog from lambdoid prophage e14 (fragment)	29%	*yadL* ←	putative fimbrial protein
8%	*fepB* ← / → *entC*	ferric enterobactin (enterochelin) binding protein; periplasmic component/isochorismate hydroxymutase 2, enterochelin biosynthesis	20%	*bax* ←	putative ATP-binding protein
			16%	*ycgM* →	putative isomerase
			15%	*gatA* ←	galactitol-specific enzyme IIA of phosphotransferase system
8%	*yadL* ←	putative fimbrial protein	14%	*yhdZ* → / ← *rrfF*	putative ATP-binding component of a transport system/5S ribosomal RNA
6%	*yadL* ←	putative fimbrial protein	11%	*ptsP* ←	PTS system, enzyme I, transcriptional regulator (with NPR and NTR proteins)
6%	*flu* → / → *yeeR*	antigen 43, phase-variable bipartite outer membrane fluffing protein/orf, hypothetical protein	9%	*frmR* ← / ← *yaiO*	repressor of *frmRAB*/orf, hypothetical protein
5%	*hemN* → / ← *glnG*	O2-independent coproporphyrinogen III oxidase/response regulator for gln (sensor glnL) (nitrogen regulator I, NRI)	9%	*yciQ* →	orf, hypothetical protein
			8%	*ptsP* ←	PTS system, enzyme I, transcriptional regulator (with NPR

			and NTR proteins)
	7%	*ogrK* ←	prophage P2 ogr protein
	6%	*yiaN* →	putative membrane protein
	5%	*ycfK* →	hypothetical protein in lambdoid prophage e14 region
	5%	*aroM* →	protein of *aro* operon

4.3 Model and generalization

Inspired by the experimental observation, the following population genetic model is built to generalize the effect of trade-off on adaptation. In the context of population genetics, the presence of a biological trade-off means the distribution of beneficial mutations is skewed to the low end and the Pareto front demarks a boundary beyond which possible genotypes become exceedingly rare, assuming they still exist. This is a critical premise for the model.

Now we can calculate the rate of adaptation, defined by the rate it takes for the mutant with highest fitness to sweep the population, while varying skewness of the distribution of beneficial mutations. The result is shown in **Fig. 22**. Surprisingly, distributions with higher kurtosis (a statistical measure of skewness) produces faster adaptation. Higher kurtosis can be interpreted as more severe trade-off. Without any specification of the details and mechanisms of trade-off, its "generative effect" on adaptation naturally emerges as the consequence of a simple population genetic process.

Intuition of this effect lies on the fact that, by skewing the distribution of beneficial mutations to lower fitness, trade-off effectively reduces clonal interference at

the regime of high fitness mutants. In other words, with fewer possible competitors of close but lower fitness in the population, the mutant carrying the best beneficial mutation shall sweep the population faster. Since this mutation is rare and has not been realized before, the probability that it comes with a novel solution to overcome the trade-off increases. In the context of the empirical observation discussed before, the novel solution is the reprogramming of swimming speed kinetics that changed the life style of the organism.

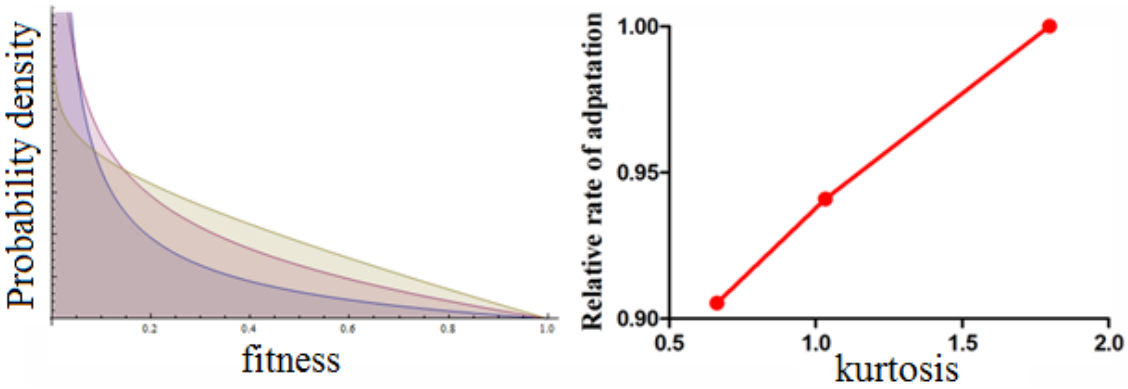

Figure 22 | Adaptation rate for distributions of beneficial mutations with different kurtosis values. The model is based on a Moran model with a fixed population size of 2000 individuals. Evolution starts with a pure population of wild type and proceeds with repeated rounds of birth, death and mutation. At each round, a individual is selected for birth (increase by 1). The probability of being selected for each type of mutant/wild type is proportional to their own fitness weighted by its abundance in the population. Then, an individual is randomly chosen for death (decrease by 1). Lastly, a wild type individual is chose to mutate. The type of mutant it changes to is a random process biased by the frequency of each possible mutant so that a frequent mutant is more likely to be realized. The continuous distributions of beneficial mutations on the left were discretized by 1000 samplings each and then used in the simulation of evolution. Rates of adaptation is normalized to the rate from the distribution with the highest kurtosis.

Trade-off is usually associated with constraints that hinder organism's functional capability(Behrends et al., 2014; Chandra et al., 2011; Dessau et al., 2012; Lan et al., 2012; Mole and Zera, 1993; Shoval et al., 2012; Tokuriki et al., 2012). However, it is

exactly the same restrictive conditions that also lead to relentless exploration in the space of alternative solutions via the ingenious selection-mutation interaction (Keen, 2014; Phan and Ferenci, 2013). Biological complexities, i.e., the realized ways around the trade-off, naturally spin off from this process. Here, I demonstrate this generative effect of trade-off with an example elucidated in both evolutionary and physiological mechanisms. Our work demonstrated the flexibility of bacterial genomes to rapidly generate novelty, driven by intrinsic limit, to precisely adapt to sophisticated selective regimes. The illuminated molecular underpinnings of motility reprogramming provides insight to the evolution of physiological regulation, a central theme for the diverse lifestyles found among microbial pathogens (Ohm et al., 2012). By emphasizing the generative effect of trade-off, this study enriches to our general thoughts on the emergence of biological complexity.

References

Acar, M., Mettetal, J.T., and van Oudenaarden, A. (2008). Stochastic switching as a survival strategy in fluctuating environments. Nat Genet *40*, 471-475.

Agrawal, A.A., Conner, J.K., and Rasmann, S. (2010). Tradeoffs and negative correlations in evolutionary ecology. In Evolution since Darwin: the first 150 years, M. Bell, D. Futuyma, W. Eanes, and J. Levinton, eds. (Sunderland, MA: Sinauer Associates, Inc.).

Allouche, O., Kalyuzhny, M., Moreno-Rueda, G., Pizarro, M., and Kadmon, R. (2012). Area–heterogeneity tradeoff and the diversity of ecological communities. Proc Natl Acad Sci USA *109*, 17495-17500.

Amarasekare, P. (2003). Competitive coexistence in spatially structured environments: a synthesis. Ecol Lett *6*, 1109-1122.

Amsler, C.D., Cho, M., and Matsumura, P. (1993). Multiple factors underlying the maximum motility of Escherichia coli as cultures enter post-exponential growth. J Bacteriol *175*, 6238-6244.

ARNOLD, S.J. (1983). Morphology, performance and fitness. Am Zool *23*, 347-361.

Barker, C.S., Prüß, B.M., and Matsumura, P. (2004). Increased motility of *Escherichia coli* by insertion sequence element integration into the regulatory region of the flhD operon. J Bacteriol *186*, 7529-7537.

Barrick, J.E., Yu, D.S., Yoon, S.H., Jeong, H., Oh, T.K., Schneider, D., Lenski, R.E., and Kim, J.F. (2009). Genome evolution and adaptation in a long-term experiment with *Escherichia coli*. Nature *461*, 1243-1247.

Beaumont, H.J.E., Gallie, J., Kost, C., Ferguson, G.C., and Rainey, P.B. (2009). Experimental evolution of bet hedging. Nature *462*, 90-93.

Behrends, V., Maharjan, R.P., Ryall, B., Feng, L., Liu, B., Wang, L., Bundy, J.G., and Ferenci, T. (2014). A metabolic trade-off between phosphate and glucose utilization in *Escherichia coli*. Mol BioSyst *10*, 2820-2822.

Bell, G. (2010). Fluctuating selection: the perpetual renewal of adaptation in variable environments. Phil Trans R Soc B *365*, 87-97.

Berenbaum, M.R., Zangerl, A.R., and Nitao, J.K. (1986). Constraints on chemical coevolution: wild parsnips and the parsnip webworm. Evolution *40*, 1215-1228

Boehm, A., Kaiser, M., Li, H., Spangler, C., Kasper, C.A., Ackermann, M., Kaever, V., Sourjik, V., Roth, V., and Jenal, U. (2010). Second messenger-mediated adjustment of bacterial swimming velocity. Cell *141*, 107-116.

Brittain, J.E., and Campbell, I.C. (1991). The effect of temperature on egg development in the australian mayfly genus coloburiscoides (ephemeroptera: coloburiscidae) and its relationship to distribution and life history. J Biogeogr *18*, 231-235.

Cáceres, C.E. (1997). Temporal variation, dormancy, and coexistence: A field test of the storage effect. Proc Natl Acad Sci USA *94*, 9171-9175.

Chandra, F.A., Buzi, G., and Doyle, J.C. (2011). Glycolytic oscillations and limits on robust efficiency. Science *333*, 197-192.

Chesson, P. (2000). Mechanisms of maintenance of species diversity Annu Rev Ecol Evol Syst *31*, 343-366.

Chesson, P., and Huntly, N. (1993). Temporal hierarchies of variation and the maintenance of diversity. Plant Spec Biol *8*, 195-206.
Chesson, P.L. (1983). Coexistence of competitors in a stochastic environment: the storage effect. Lect Notes Biomath *52*, 188-198.
Codeço, C.T., and Grover, J.P. (2001). Competition along a spatial gradient of resource supply: a microbial experimental model. Am Nat *157*, 300-315.
Cohen, D. (1966). Optimizing reproduction in a randomly varying environment. J Theor Biol *12*, 119-129.
Datsenko, K.A., and Wanner, B.L. (2000). One-step inactivation of chromosomal genes in *Escherichia coli* K-12 using PCR products. Proc Natl Acad Sci USA *97*, 6640-6645.
Dean, A.M. (2005). Protecting haploid polymorphisms in temporally variable environments. Genetics *169*, 1147-1156.
Dempster, E.R. (1955). Maintenance of genetic heterogeneity. Cold Spring Harbor Symp Quant Biol, 25-32.
Dessau, M., Goldhill, D., McBride, R., Turner, P.E., and Modis, Y. (2012). Selective pressure causes an RNA virus to trade reproductive fitness for increased structural and thermal stability of a viral enzyme. PLoS Genet *8*, 29.
Domínguez, M., Moreno, I., Aizpurua, C., and Toraño, A. (2003). Early mechanisms of Leishmania infection in human blood. Microb Infect *5*, 507-513.
Dykhuizen, D.E., and Dean, A.M. (1990). Enzyme activity and fitness: Evolution in solution. Trends Ecol Evol *5*, 257-262.
Edelaar, P. (2013). Comment on "Evolutionary Trade-Offs, Pareto Optimality, and the Geometry of Phenotype Space". Science *339*, 757.
Eldar, A., and Elowitz, M.B. (2010). Functional roles for noise in genetic circuits. Nature *467*, 167-173.
Felsenstein, J. (1976). The theoretical population genetics of variable selection and migration. Annu Rev Genet *10*, 253-280.
Frank, S.A., and Slatkin, M. (1990). Evolution in a variable environment. Am Nat *136*, 244-260.
Freter, R., and O'Brien, P.C. (1981). Role of chemotaxis in the association of motile bacteria with intestinal mucosa: chemotactic responses of *Vibrio cholerae* and description of motile nonchemotactic mutants. Infect Immu *34*, 215-221.
Friedland, A.E., Lu, T.K., Wang, X., Shi, D., Church, G., and Collins, J.J. (2009). Synthetic gene networks that count. Science *324*, 1199-1202.
Gardner, T.S., Cantor, C.R., and Collins, J.J. (2000). Construction of a genetic toggle switch in *Escherichia coli*. Nature *403*, 339-342.
Gerland, U., and Hwa, T. (2009). Evolutionary selection between alternative modes of gene regulation. Proc Natl Acad Sci USA *106*, 8841-8846.
Gillespie, J.H. (1972). The effects of stochastic environments on allele frequencies in natural populations. Theor Pop Biol *3*, 241-248.
Gliddon, C., and Strobeck, C. (1975). Necessary and sufficient conditions for multiple-niche polymorphism in haploids. Am Nat *109*, 233-235.
Gotelli, N.J. (2008). A Primer of Ecology, 4 edn (Sinauer Associates, Inc., MA).

Haldane, J., and Jayakar, S. (1963). Polymorphism due to selection of varying direction. J Genet *58*, 237-242.
Hartl, D.L., and Cook, R.D. (1974). Autocorrelated random environments and their effects on gene frequency. Evolution *28*, 275-280.
Heino, M., Metz, J.A.J., and Kaitala, V. (1998). The enigma of frequency-dependent selection. Trends Ecol Evol *13*, 367-370.
Hurme, R., and Rhen, M. (1998). Temperature sensing in bacterial gene regulation — what it all boils down to. Mol Microbiol *30*, 1-6.
Hutchinson, G.E. (1961). The paradox of the plankton. Am Nat *95*, 137-145.
Jacob, F., and Monod, J. (1961a). Genetic regulatory mechanisms in the synthesis of proteins. J Mol Biol *3*, 318-356.
Jacob, F., and Monod, J. (1961b). On the regulation of gene activity. Cold Spring Harbor Sym Quant Biol *26*, 193-211.
Kaern, M., Elston, T.C., Blake, W.J., and Collins, J.J. (2005). Stochasticity in gene expression: from theories to phenotypes. Nat Rev Genet *6*, 451-464.
Karlin, S., and Liberman, U. (1975). Random temporal variation in selection intensities: One-locus two-allele model. J Math Biol *2*, 1-17.
Keen, E.C. (2014). Tradeoffs in bacteriophage life histories. Bacteriophage *4*, e28365.
Keller, R.A., Peeters, C., and Beldade, P. (2014). Evolution of thorax architecture in ant castes highlights trade-off between flight and ground behaviors Elife *3*, e01539.
Kimura, M. (1954). Process leading to quasi-fixation of genes in natural populations due to random fluctuation of selection intensities. Genetics *39*, 280-295.
Kimura, M. (1983). The neutral theory of molecular evolution (Cambrige University).
Kleiber, M. (1947). Body size and metabolic rate. Physiol Rev *27*, 511-541.
Koirala, S., Mears, P., Sim, M., Golding, I., Chemla, Y.R., Aldridge, P.D., and Rao, C.V. (2014). A nutrient-tunable bistable switch controls motility in salmonella enterica serovar typhimurium. mBio *5*, e1611-1614.
Kussell, E., and Leibler, S. (2005). Phenotypic diversity, population growth, and information in fluctuating environments. Science *309*, 2075-2078.
Lan, G., Sartori, P., Neumann, S., Sourjik, V., and Tu, Y. (2012). The energy-speed-accuracy trade-off in sensory adaptation. Nat Phys *8*, 422-428.
Lebreton, B., Prasad, P.V., Jayaram, M., and Youderian, P. (1988). Mutations that improve the binding of yeast flp recombinase to its substrate. Genetics *118*, 393-400.
Lenski, R.E. Relative fitness: its estimation and its significance for environmental applications of microorganisms, in Microbial Ecology: Principles, Methods, and Applications, M. A. Levin, R. J. Seidler and M. Rogul, eds. (McGraw-Hill Book Co., New York).
Lenski, R.E., and Travisano, M. (1994). Dynamics of adaptation and diversification: a 10,000-generation experiment with bacterial populations. Proc Natl Acad Sci USA *91*, 6808-6814.
Levene, H. (1953). Genetic equilibrium when more than one ecological niche is available. Am Nat *87*, 331-333.
Levin, R. (1968). Evolution in Changing Environments (NJ: Princeton University).

Levin, S.A.a.H.C.M.-L. (2000). The evolution of dispersal and seed size in plant communities. Evol Ecol Res 409-435.
Levy, S.F., Ziv, N., and Siegal, M.L. (2012). Bet hedging in yeast by heterogeneous, age-correlated expression of a stress protectant. PLoS Biol *10*, 8.
Lopilato, J.E., Garwin, J.L., Emr, S.D., Silhavy, T.J., and Beckwith, J.R. (1984). D-ribose metabolism in *Escherichia coli* K-12: genetics, regulation, and transport. J Bacteriol *158*, 665-673.
Lunzer, M., Natarajan, A., Dykhuizen, D.E., and Dean, A.M. (2002). Enzyme kinetics, substitutable resources and competition: from biochemistry to frequency-dependent selection in *lac*. Genetics *162*, 485-499.
Macnab, R.M. (1996). Flagella and Motility (Washington, DC: ASM Press).
May, R.M. (1973). Stability and Complexity in Model Ecosystems (NY: Princeton University Press).
Mayr, E. (1961). Cause and effect in biology. Science *134*, 1501-1506.
Messina, F.J., and Fox, C.W. (2001). Offspring size and number. In Evolutionary Ecology: Concepts and Case Studies, C.W. Fox, D.A. Roff, and D.J. Fairbairn, eds. (New York: Oxford University Press).
Miller, J. (1992). A Short Course in Bacterial Genetics (Plainview, NY: Cold Spring Harbor Lab. Press).
Mitchell-Olds, T.a.W., John H (2007). Which evolutionary processes influence natural genetic variation for phenotypic traits? Nat Rev Genet *8*, 845-856.
Mole, S., and Zera, A. (1993). Differential allocation of resources underlies the dispersal-reproduction trade-off in the wing-dimorphic cricket, *Gryllus rubens*. Oecologia *93*, 121-127.
Nagrath, D., Avila-Elchiver, M., Berthiaume, F., Tilles, A., Messac, A., and Yarmush, M. (2007). Integrated energy and flux balance based multiobjective framework for large-scale metabolic networks. Ann Biomed Eng *35*, 863-885.
Ohm, R.A., Feau, N., Henrissat, B., Schoch, C.L., Horwitz, B.A., Barry, K.W., Condon, B.J., Copeland, A.C., Dhillon, B., Glaser, F., *et al.* (2012). Diverse lifestyles and strategies of plant pathogenesis encoded in the genomes of eighteen *dothideomycetes* fungi. PLoS Pathog *8*, e1003037.
Pake, C.E., and Venable, D.L. (1996). Seed banks in desert annuals: implications for persistence and coexistence in variable environments. Ecology *77*, 1427-1435.
Pesavento, C., Becker, G., Sommerfeldt, N., Possling, A., Tschowri, N., Mehlis, A., and Hengge, R. (2008). Inverse regulatory coordination of motility and curli-mediated adhesion in *Escherichia coli*. Genes Dev *22*, 2434-2446.
Phan, K., and Ferenci, T. (2013). A design-constraint trade-off underpins the diversity in ecologically important traits in species *Escherichia coli*. ISME J *7*, 2034-2043.
Philippi, T. (1993). Bet-hedging germination of desert annuals: beyond the first year. The Am Nat *142*, 474-487.
Poelwijk, Frank J., de Vos, Marjon G.J., and Tans, Sander J. (2011). Tradeoffs and optimality in the evolution of gene regulation. Cell *146*, 462-470.
Rose, M.R., and Charlesworth, B. (1981). Genetics of life history in *Drosophila melanogaster*. II. Exploratory selection experiments. Genetics *97*, 187-196.

Sambrook, J.a.R., D. W. (2001). Molecular Cloning: A Laboratory Manual (NY: Cold Spring Harbor Laboratory Press).
Santillán, M., Mackey, M.C., and Zeron, E.S. (2007). Origin of bistability in the lac operon. Biophys J *92*, 3830-3842.
Schoener, T.W. (1974). Resource partitioning in ecological communities. Science *185*, 27-39.
Shahrezaei, V., and Swain, P.S. (2008). The stochastic nature of biochemical networks. Curr Opin Biotechnol *19*, 369-374.
Shoval, O., Sheftel, H., Shinar, G., Hart, Y., Ramote, O., Mayo, A., Dekel, E., Kavanagh, K., and Alon, U. (2012). Evolutionary trade-offs, pareto optimality, and the geometry of phenotype space. Science *336*, 1157-1160.
Siepielski, A.M., and McPeek, M.A. (2010). On the evidence for species coexistence: a critique of the coexistence program. Ecology *91*, 3153-3164.
Simon, A.L. (1976). Population dynamic models in heterogeneous environments. Annual Rev Ecol Syst *7*, 287-310.
Simons, A.M. (2009). Fluctuating natural selection accounts for the evolution of diversification bet hedging. Proc R Soc B: Biol Sci *276*, 1987-1992.
Sorenson, M.K., Ray, S.S., and Darst, S.A. (2004). Crystal structure of the flagellar σ/anti-σ complex σ28/flgm reveals an intact σ factor in an inactive conformation. Mol Cell *14*, 127-138.
Staropoli, J.F., and Alon, U. (2000). Computerized analysis of chemotaxis at different stages of bacterial growth. Biophys J *78*, 513-519.
Starrfelt, J., and Kokko, H. (2012). Bet-hedging—a triple trade-off between means, variances and correlations. Biol Rev *87*, 742-755.
Stewart, F.M., and Levin, B.R. (1973). Partitioning of resources and the outcome of interspecific competition: a model and some general considerations. Am Nat *107*, 171-198.
Suiter, A.M., Bänziger, O., and Dean, A.M. (2003). Fitness consequences of a regulatory polymorphism in a seasonal environment. Proc Natl Acad Sci USA *100*, 12782-12786.
Szewczyk, E., Nayak, T., Oakley, C.E., Edgerton, H., Xiong, Y., Taheri-Talesh, N., Osmani, S.A., and Oakley, B.R. (2007). Fusion PCR and gene targeting in Aspergillus nidulans. Nat Protocols *1*, 3111-3120.
Tamme, R., Hiiesalu, I., Laanisto, L., Szava-Kovats, R., and Pärtel, M. (2010). Environmental heterogeneity, species diversity and co-existence at different spatial scales. J Veget Sci *21*, 796-801.
Tan, C., Reza, F., and You, L. (2007). Noise-limited frequency signal transmission in gene circuits. Biophys J *93*, 3753-3761.
Taniguchi, Y., Choi, P.J., Li, G.-W., Chen, H., Babu, M., Hearn, J., Emili, A., and Xie, X.S. (2010). Quantifying e. coli proteome and transcriptome with single-molecule sensitivity in single cells. Science *329*, 533-538.
Thattai, M., and van Oudenaarden, A. (2004). Stochastic gene expression in fluctuating environments. Genetics *167*, 523-530.

Tinbergen, N. (1963). On aims and methods of ethology. Zeitschrift für Tierpsychologie *20*, 410-433.

Tokuriki, N., Jackson, C.J., Afriat-Jurnou, L., Wyganowski, K.T., Tang, R., and Tawfik, D.S. (2012). Diminishing returns and tradeoffs constrain the laboratory optimization of an enzyme. Nat Commun *3*, 1275.

Toprak, E., Veres, A., Michel, J.-B., Chait, R., Hartl, D.L., and Kishony, R. (2012). Evolutionary paths to antibiotic resistance under dynamically sustained drug selection. Nat Genet *44*, 101-105.

Turelli, M., and Gillespie, J.H. (1980). Conditions for the existence of stationary densities for some two-dimensional diffusion processes with applications in population biology. Theor Pop Biol *17*, 167-189.

Turelli, M., Schemske, D.W., and Bierzychudek, P. (2001a). Stable two-allele polymorphisms maintained by fluctuating fitnesses and seed banks: protecting the blues in *linanthus parryae*. Evolution *55*, 1283-1298.

Veening, J.-W., Stewart, E.J., Berngruber, T.W., Taddei, F., Kuipers, O.P., and Hamoen, L.W. (2008). Bet-hedging and epigenetic inheritance in bacterial cell development. Proc Natl Acad Sci USA *105*, 4393-4398.

Wang, H.H., Isaacs, F.J., Carr, P.A., Sun, Z.Z., Xu, G., Forest, C.R., and Church, G.M. (2009). Programming cells by multiplex genome engineering and accelerated evolution. Nature *460*, 894-898.